GRADUATE AERONAUTICAL LABORATORIES
CALIFORNIA INSTITUTE OF TECHNOLOGY

An Experimental Investigation of the Failure of a Stepped Composite Plate

Thesis by
Steven C. Gortsema

Aeronautical Engineer

Research Supported by the Air Force Office of Scientific Research
and by NASA Grant NSG 1483

SM 91-10

Firestone Flight Sciences Laboratory

Guggenheim Aeronautical Laboratory

Karman Laboratory of Fluid Mechanics and Jet Propulsion

Pasadena

REPORT DOCUMENTATION PAGE

AFRL-SR-BL-TR-98-

0727

1. AGENCY USE ONLY (Leave Blank)	2. REPORT DATE	3. REPORT TYPE AND DATES COVERED
	1992	Final

4. TITLE AND SUBTITLE	5. FUNDING NUMBERS
An Experimental Investigation of the Failure of a Stepped Composite Plate	
6. AUTHORS Steven C. Gortsema	
7. PERFORMING ORGANIZATION NAME(S) AND ADDRESS(ES) California Institute of Technology	8. PERFORMING ORGANIZATION REPORT NUMBER
9. SPONSORING/MONITORING AGENCY NAME(S) AND ADDRESS(ES) AFOSR/NI 4040 Fairfax Dr, Suite 500 Arlington, VA 22203-1613	10. SPONSORING/MONITORING AGENCY REPORT NUMBER
11. SUPPLEMENTARY NOTES	
12a. DISTRIBUTION AVAILABILITY STATEMENT Approved for Public Release	12b. DISTRIBUTION CODE

13. ABSTRACT *(Maximum 200 words)*

See Attachment

14. SUBJECT TERMS	15. NUMBER OF PAGES
	16. PRICE CODE

17. SECURITY CLASSIFICATION OF REPORT	18. SECURITY CLASSIFICATION OF THIS PAGE	19. SECURITY CLASSIFICATION OF ABSTRACT	20. LIMITATION OF ABSTRACT
Unclassified	Unclassified	Unclassified	UL

An Experimental Investigation of the Failure of a Stepped Composite Plate

Thesis by

Steven C. Gortsema

In Partial Fulfillment of the Requirements for the Degree of

Aeronautical Engineer

Research Supported by the Air Force Office of Scientific Research

and by NASA Grant NSG 1483

California Institute of Technology

Pasadena, California

1992

(Submitted September 6, 1991)

To my wife, my parents, and my brother,

for all of their love and support.

Acknowledgements

I am very grateful to the Air Force Office of Scientific Research for awarding a generous fellowship to me. In particular, I wish to thank Majors Stephen Whitehouse and Al Janiszewski, who were my fellowship mentors, and Professor Warren Peele, the fellowship program director, for their understanding and support.

I would like to thank my advisor, Professor W.G. Knauss, for his guidance and numerous helpful suggestions throughout the course of this study. I especially wish to thank Professor Knauss for his invaluable assistance in the preparation of this thesis. Also, I have learned a great deal from Professor G. Ravichandran. His patient assistance is much appreciated.

I would like to thank Allen Waters, Dr. J. Starnes, and Mark Shuart at NASA Langley for providing the specimens used in this study. I am also grateful to George Lundgren and Phil Wood, from the Aero shop, for the use of their equipment and for their cheerful assistance in fabricating the experimental apparatus. The help of Jean Anderson, from the Aero library, is also appreciated. The C-scans were performed by Kelly Brown and Bill Glass at Sonic Testing and Engineering. I thank them for their time and for the use of their facilities.

Finally, special thanks go to my friends and colleagues of the Solid Mechanics Group. In particular, the assistance of Guillaume Vendroux is acknowledged. His experience with composite materials and with polishing was very helpful in the early stages of the experimental work.

Abstract

The progression of damage in a stepped composite plate has been investigated experimentally. This study is intended to provide insight into the failure behavior of co-cured, stringer-reinforced composite plates and shells. The specimens were constructed of four different lay-ups of carbon-fiber-reinforced epoxy and were subjected to various combinations of moment, tension, and shear static loadings.

The primary means of damage observation was *in situ* microscopic inspection of the specimen edges. These observations were supplemented by penetrant-dye inspection, microscopic inspection of the plate face, and ultrasonic C-scanning of specimens which were unloaded prior to catastrophic failure. In addition to providing detailed descriptions of the damage development, this thesis presents hypotheses which attempt to explain the mechanisms involved in the failure process.

The immediate goal of this work was to gather the experimental evidence needed to evaluate a recently proposed failure criterion. The criterion attempts to predict failure for an arbitrary lay-up by studying the behavior of the computed stresses within an extremely small vicinity of the singularity. The tests described in this thesis revealed that damage initiation does not always occur on the plate–stringer interface, as assumed in the failure criterion. Furthermore, it was discovered that in some lay-ups, damage initiates at a distance of over one lamina thickness away from the singularity. This fact makes it impossible to predict failure accurately with *any* criterion which is based solely on a computed stress singularity.

Table of Contents

List of Figures

List of Tables

1. Introduction

The widespread use of composite structures has provided engineers with a plethora of design challenges over the past few decades and will continue to do so for many years to come. One topic of considerable importance in structural designs is that of co-cured, stringer-reinforced composite plates and shells. These structures have proven themselves to be a very efficient means of constructing parts such as wing and fuselage skins. When the plates or shells are subjected to buckling loads, they often maintain considerable strength well into the post-buckling regime. Ultimate failure is then controlled largely by the local failure of the stiffener–panel connection. By co-curing the stringers onto the plate, excellent bonding can be achieved, allowing the part to support very high loads.

When a stringer-reinforced plate does fail, the failure often occurs where the edge of the stringer flange intersects the plate face (Figure 1).

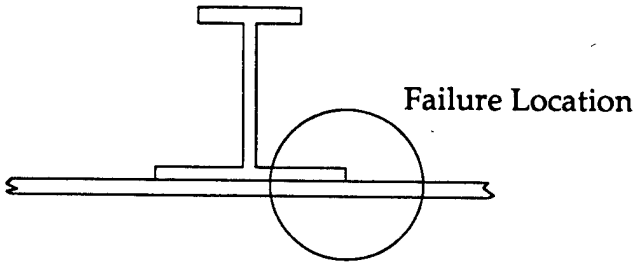

Figure 1. End view of stringer on plate.

The damage initiation is associated with the stress concentration near the re-entrant corner found along this line of intersection. However, the details of the failure process are not well understood. It is not clear why some lay-ups

allow the stringers to peel away more easily than others. In order to design more efficient structures, it is, therefore, of paramount importance to develop a detailed understanding of the mechanisms involved in this type of failure.

The present study contributes to this endeavor by experimentally investigating the failure in a stepped composite plate under various static loadings (Figure 2).

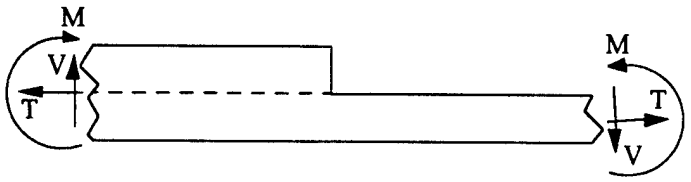

Figure 2. Geometry of the problem studied.

By using the simpler geometry of this generic problem, one can learn about many of the same mechanisms that are involved in the failure of the stiffener–plate interface shown in Figure 1. The primary objective of this study is to provide a detailed description of the failure process for each lay-up tested in order to obtain a better understanding of the damage development in more complex structures. One application of this increased understanding is the ability to provide more accurate diagnoses regarding the safety of damaged parts: If it is known that before a part fails, it must exhibit additional features in its damage development, which occur stably and are detectable, then it is probably safe to continue using the part, provided its damage is closely monitored. Of even greater benefit is the application of this understanding to the design of safer, more efficient structures.

Although this thesis is only one step toward the achievement of these goals, it does have immediate applications in determining the utility of both

numerical and analytical work with regard to this problem. A recent study by Kubr [1990]* used finite element analysis to characterize the stress singularity for various stacking sequences of the geometry studied here. Kubr used a plane-coupled strain† formulation of the problem to calculate the stresses caused by moment, tension, and shear loadings applied at the step. Each lamina was homogenized for this calculation. Similar to the Williams solution at a crack tip [1952], the stresses were then assumed to be of the form $\sigma = \Psi r^{-k}$, where Ψ is called the intensity coefficient and k is called the severity of the singularity. However, here both Ψ and k are functions of θ, the angular component of the polar coordinate system centered at the corner. By using a very fine finite-element mesh near the singularity, plots of $\log(\sigma)$ vs. $\log(r)$ were generated for each stress component along four rays originating at the corner.** A linear fit to these plots provides $-k$, the slope, and $\log(\Psi)$, the intercept. Thus, for each stress component the intensity coefficient and severity of the singularity are calculated along each ray for the three loading types considered (pure moment, pure tension, and pure shear). This process is repeated for several different lay-ups.

Kubr also proposed a failure criterion based on this singularity characterization. He assumed that failure would occur on the plate–stringer interface near the corner. He then suggested that by comparing the intensity coefficient of the interlaminar tensile stress on this interface with some critical value, one could predict when a specimen would fail. This criterion

* Brackets refer to references listed in the back of the thesis. When the authors' names are obvious, only the years of publication are included in the brackets.

† Orthotropic materials in general exhibit coupling between the in-plane and out-of-plane components of stress and strain. Plane-coupled strain is a two-dimensional, linearized analysis, which accounts for these coupling effects by allowing out-of-plane displacements. The interested reader can consult Kubr's thesis for the details of this theory.

** The rays used correspond to the $\pm x$ and $\pm z$ axes shown in Figure 4.

implies that the failure process is dominated by singularity-related stresses in an extremely small domain near the (idealized) corner, dimensions that are small compared even to the lamina thickness. Thus doubt arises as to whether a continuum analysis as performed by Kubr can lead to reasonable physical interpretations. The present study, which was conceived as the experimental counterpart to Kubr's work, provides experimental evidence needed to evaluate his criterion as well as others that may be developed in the future. It is of interest in the present context to state that the experimental failure process involves a space domain which is very much larger than the singularity domain established in Kubr's work.

2. Specimens

Before the specific specimens used in this study are discussed, it is appropriate to consider first the effects of free edges on composite materials. Recall that when a material interface (a common boundary along which two distinct materials are perfectly bonded) intersects a geometric interface (such as a free edge), the theoretical stresses are singular along the line of intersection [Bogy, 1968]. The boundary layer in which these singular stresses are important in composites is approximately the size of one ply thickness. However, these effects can be significant under both static and fatigue failure conditions for these materials, making the modeling of a composite structure more difficult since specimens with free edges contain damage initiation sites that may not exist on the actual part. Therefore, if it is not possible to eliminate free-edge effects totally in an experiment, then it is best to find a way to keep the damage initiated by these effects localized to the edges, thus preventing it from having a significant effect on the global load-bearing capabilities of the specimen.

Likewise, in the current experiment, one needs to consider how the specimens or loading apparatus can be designed to ensure that free edges do not significantly influence the damage development. One way in which this goal can be achieved is to use wide plates which are stitched along the edges to prevent the free-edge delaminations from spreading to the interior of the specimen [Mignery, Tan, and Sun, 1985]. Provided the plates were wide enough, this specimen design would allow the damage to develop in the middle region of the specimen as if there were no free-edge effects. However,

this would add considerable cost and complexity to the experiment. Not only would the specimens be very expensive to manufacture, but any type of damage evaluation which relies on inspection of the free edges would not be applicable. For these reasons, it was decided to use simple beam-type specimens for this study. This decision obviously allowed the free edges to influence the damage development. However, it was expected that many of the same damage mechanisms involved in the failure of application-type geometries would also be exhibited in the simpler specimens. Therefore, an analysis of their damage development should provide some significant insight into the failure of a stepped plate without free edges.

The specimens used in this study were constructed of AS4/3502 carbon-fiber-reinforced epoxy† and were provided by Dr. Starnes and co-workers at NASA's Langley Research Center. This material was selected because of its availability and its widespread use in the aerospace industry. The specimen geometry is shown in Figure 3* :

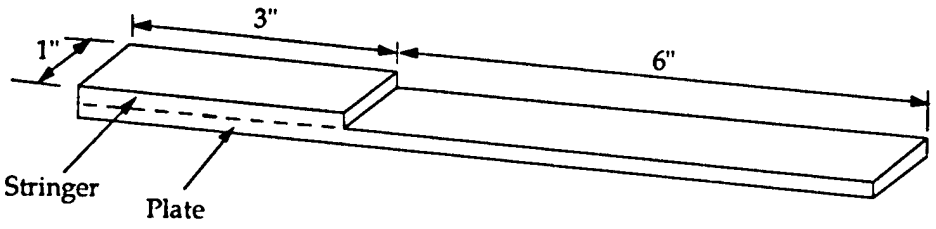

Figure 3. Specimen geometry.

† The material properties are listed in Table 4, which is found on page 84 of the appendix.
* The thicknesses are not specified in the figure because they depend on the number of plies, which is not the same for all lay-ups. However, the most common number of plies is 8 for the plate plus 8 for the stringer. These specimens have thicknesses of .040" (1 mm) on the thin side of the plate and .080" (2 mm) on the thick side.

All of the specimens for each lay-up were fabricated as a single, stepped plate, which was then cut into individual specimen strips after the curing/cooling cycle was completed. The thicker portion of the plate, which will be referred to as the stringer, was co-cured with the base plate. After the specimens were cut, each one was C-scanned to ensure that no delaminations, voids, nor inclusions were present.

Before this experimental study was started, it was believed that the failure process of all lay-ups would be dominated by the character of the theoretical stress singularity at the re-entrant corner. Furthermore, by comparing various features of this singularity for different stacking sequences, it was expected that one could predict the relative load levels at which each lay-up would fail. This concept implied that composite structures containing singularities could be optimized in terms of their ability to resist failure, as well as in their characteristics of stiffness and strength away from the discontinuity. The optimization process could be as simple as a comparison of the intensity coefficients for the opening stress on the plate-stringer interface (Kubr's postulated failure criterion), or perhaps it would be a more complex relation involving several characteristics of the singularity. This experimental study was intended to clarify which features of the singularity, if any, were most important in determining the failure of a particular lay-up. Therefore, the choice of lay-ups used in this study was guided by Kubr's numerical work, which characterized the singularity for several different lay-ups.

It was desired to select from Kubr's study those stacking orders which were associated with significantly different characteristics of the singularity, but which also had enough similarity in their lay-ups to allow critical features to be identified, e.g., certain intensity coefficients, plate thickness, step ratio, interface plies, symmetries, percentage of ±45° plies, etc. The four different lay-ups selected (out of the 23 examined by Kubr), as well as the number of specimens tested for each case, are shown in Table 1. The orientation of each ply is listed in the order it is layed up, from bottom to top in Figure 3, and the subscript S refers to a symmetric lay-up. As an example, the plate lay-up for case 1 is written explicity as [90, +45, 0, -45, -45, 0, +45, 90].

Case	Plate Lay-up	Stringer Lay-up	Number of Tests
1	$[90, +45, 0, -45]_S$	$[90, +45, 0, -45]_S$	5
2	$[+45, 0, -45, 90]_S$	$[+45, 0, -45, 90]_S$	6
3	$[90, 0, -45, +45]_S$	$[0, -45, +45, 90_2]$	5
4	$[90_2, +45_2, 0_2, -45_2]_S$	$[90_2, +45_2, 0_2, -45_2]_S$	2

Table 1. Lay-up description for specimens examined.

The ply orientations are specified in terms of the coordinate system shown in Figure 4. The 0° plies contain fibers aligned with the longitudinal axis of the specimen, and positive angles are measured from the $+x$ axis toward the $+y$ axis as shown.

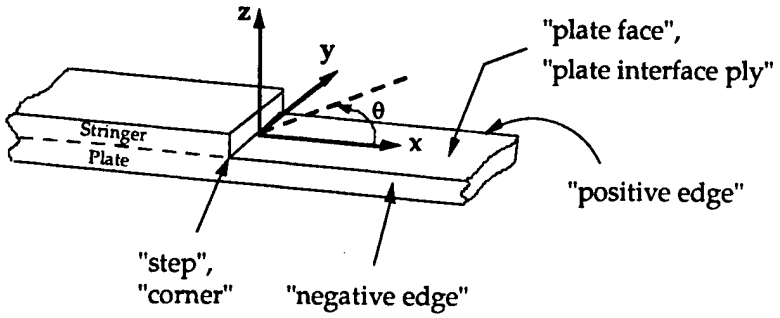

Figure 4. Coordinate system and naming convention.

This coordinate system will be used throughout the remainder of this thesis as the damage development is described. Names have been assigned to certain features of the specimen in accordance with figure 4 to simplify descriptions involving the geometry. A distinction is made between the two edges because the presence of +45° and -45° plies causes the state of stress on one edge to be different from that on the other. This observation is most easily understood by considering a 45° ply in the stringer (Figure 5).

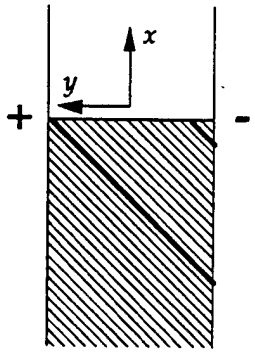

Figure 5. Asymmetric damage development.

A crack through the matrix of this ply, i.e., in the fiber direction, near the end of the step by the negative edge isolates a small, triangular section of that ply. However, a crack near the other end of the step must cross the entire width of

the specimen before part of the ply is isolated. Thus, the damage development is not symmetric about the x axis. This fact makes it desirable to refer to the two edges by different names when describing the damage process.

3. Design of the Experiment

This section is divided into 3 parts, which describe the loading apparatus, the *in situ* inspection of the damage development, and the experimental procedure.

3.1. Loading Apparatus

Since this study was conceived as an investigation of the damage progression, it was not deemed necessary to devise an elaborate loading apparatus and data collection system. All that was needed was a way to apply controllable, static loading which would satisfy the following requirements:

(i) The apparatus should provide the ability to increase the loading severity at the step by small increments; this would allow each feature in the damage process to be observed in the order in which it occurred, instead of experiencing large amounts of damage occurring simultaneously.

(ii) It was also desired to apply various combinations of moment, tension, and shear loading. By observing the damage development for several different loading combinations, one can deduce how the damage process depends on the nature of the applied loads.

(iii) The loading apparatus must leave the specimen sufficiently accessible to allow *in situ* observation of the damage development. This prevents the damage process from being affected by repeated unloading and reloading of the specimen, which otherwise accompany periodic inspections.

Also, there is no set of equations analogous to the beam equations within the theory of strength of materials which can be used to calculate the

loading near the step from various boundary conditions and known loadings at other places on the specimen. For this reason the loading apparatus must be designed in a way which allows the loadings at the step (moment, tension, and shear) to be calculated from simple force-balance principles.

The apparatus designed to accommodate the above requirements is shown in Figure 7. An aluminum tab containing a hole is glued to the plate end of each specimen to facilitate the attachment of weights. The weights are suspended from this end of the specimen, while the orientation and position of the other end are fixed. By varying the amount of weight used and the angle of the clamped end, one can achieve different combinations of moment, tension, and shear loading at the step. The only parameters that must be measured in order to calculate these loadings are the moment arm, d, and the load angle, φ (Figure 6). Once these are known, the moment (M), shear (V), and tensile (T) loadings at the step can be calculated.

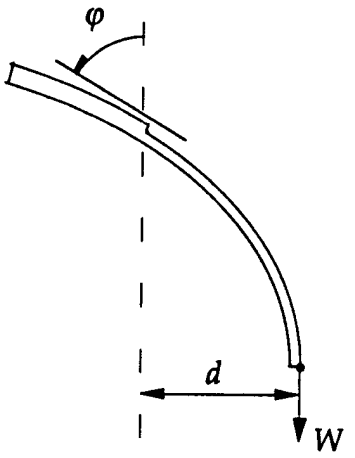

$$M = -Wd$$

$$T = W\cos\varphi$$

$$V = W\sin\varphi$$

Figure 6. The loading at the step.

Figure 7. Experimental set-up.

3.2. Inspection of the Damage Development

As mentioned previously, it was desired to find a nondestructive means of evaluating the damage development while the specimen was under load. The method selected for this task was microscopic inspection of the free edge. Although this technique revealed only the damage on the edge, its simplicity and ability to provide a detailed portrayal of the damage process in the x-z plane (Figure 4) made it preferable over other available techniques. Furthermore, the attachment of photographic equipment to the microscope allowed the recording of various features in the damage development at any time during the test.

In order to inspect the specimen as the test progressed, it was necessary to mount the microscope on a highly mobile support. This feature provided the ability to track the damage development as its position and orientation changed during the test. Although the loading fixture was designed to minimize the movement of the inspection area when the load angle, φ, was varied, the microscope support still needed 5 degrees of freedom: 2 axes of translation to follow the damage in the x-z plane; a third axis of translation to focus the image; and 2 axes of rotation to keep the microscope perpendicular to the deforming specimen, thus allowing one to focus clearly on a sufficiently large portion of the edge surface. The assembly which provided all of these abilities is shown in Figure 8.

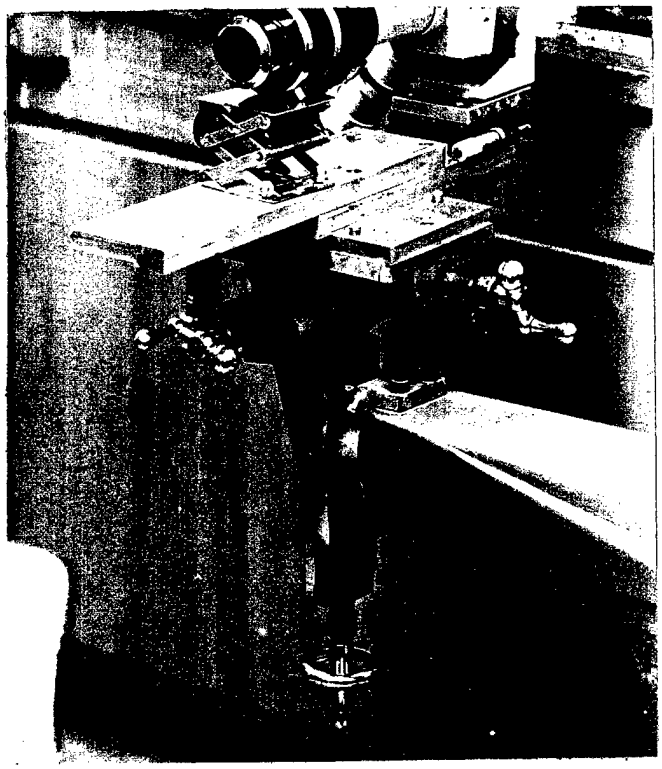

Figure 8. Microscope support.

In order to obtain an image of satisfactory resolution, it was necessary to polish the specimen edges before running a test. The polishing significantly improved the clarity of the microscopic observations. Without polishing it was difficult even to see interlaminar boundaries, but after polishing, each individual fiber was clearly visible. This specimen preparation allowed the observation of many features in the damage process that otherwise would have been undetectable.

3.3. Experimental Procedure

The testing procedure used in this experiment is quite straightforward. The stringer end of the specimen is clamped into the loading assembly. Using the microscope, an inspection is then made of the polished edge and photographs are taken of any fabrication damage or defects (if they exist). With the specimen in the vertical position ($\varphi = 0°$), a fixed amount of weight is suspended from the plate end. The load angle is then increased by small increments. After each increment, the edge of the specimen is carefully scanned for damage. Photographs are taken of any significant developments in the damage process.

At several different times during the test (usually corresponding to positions where photographs are taken), the load angle, φ, and the moment arm, d, are measured. This is done by marking the specimen orientation on a board which is rigidly attached to the loading fixture. The load angle is obtained by tracing the slope of the specimen near the step and then marking the orientation of a plumb bob which is suspended behind the corner at the base of the step. The moment arm is the distance between this plumb bob and the point at which the weight is suspended from the aluminum tab. After the photographs are taken and the specimen orientation is marked, the load angle is further increased. This process is usually continued until the specimen fails completely. By performing the tests with different amounts of weight, several different loading combinations are achieved for each lay-up case.

4. Damage Development

For the range of loading combinations (various amounts of moment, tension, and shear) considered in this experiment, the features of the damage development did not seem to be affected by varying the amount of weight used in a test. However, the damage process depended very heavily on specimen lay-up. This section, which is divided into four subsections, discusses the damage development for each lay-up case considered. The first three subsections describe the damage development in cases 1 and 4, case 2, and case 3. Cases 1 and 4 are grouped together since they exhibit the same damage mechanisms. This is not surprising since they represent the same lay-up, just on different size scales. The case 1 and 4 subsection is then divided into 3 parts. The first and second parts (Sections 4.1.1 and 4.1.2) describe the damage development as it was observed on the positive edge and the negative edge of the specimen, respectively. These sections first describe the damage as it was observed without attempting to explain any of the mechanisms involved. The third part (Section 4.1.3) then gives a more detailed account of the overall damage process and suggests some mechanisms that may explain many of the observed phenomena. The case 2 and 3 subsections are organized similar to cases 1 and 4. However, case 2 has an additional part which describes the damage as it was observed on the plate face, and case 3 combines the damage descriptions for both edges into one part. Finally, the fourth subsection presents some general ideas on how stacking sequence influences the damage process.

It should be pointed out that because of the complex nature of composite materials, it is not likely to obtain results with the same level of consistency as for materials which are commonly assumed to be isotropic and homogeneous. With composites there are many parameters that vary from one specimen to another, even when the specimens are cut from the same plate, as they were for this work. A few of these parameters are fiber volume fraction; size and position of resin-rich areas, impurities, and air bubbles; positioning of the fibers relative to each other* and relative to the step; and the existence and location of any fabrication damage. Because of this variation, the damage development was not exactly the same for every specimen of a given lay-up. However, there are a number of features which were common to the majority of the tests for each case.

4.1. Lay-up Cases 1 and 4

Let us consider first those features which are common to most of the case 1 and 4 specimens.

4.1.1. Observations on the Positive Edge

The progression of damage on the positive edge depends on the increase in the (local) load level. Each numbered step in the following sequence represents an increased load. As an example, the approximate

* Brockenbrough, Suresh, and Wienecke [1991] have performed computations on this subject for metal-matrix composites. They found that fiber distribution has a very significant effect on the deformation when the specimens are subjected to fiber-transverse loadings.

moment loadings at each step have been included for one of the specimens.* These are expressed as a percentage of the moment loading at ultimate failure for this specimen, M_{fp}. Also, to aid the reader in understanding the damage descriptions, the events which occur in each step are illustrated in Figure 9. Thus, as the loading increases on a specimen, one would trace through the following levels of damage development:

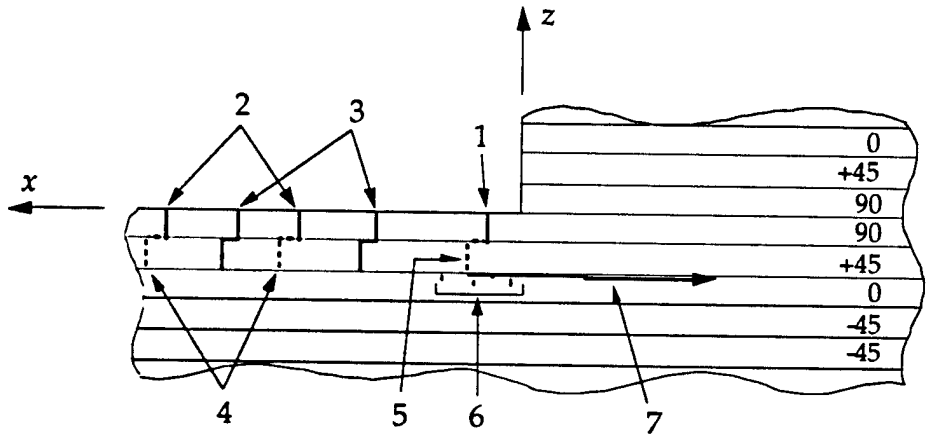

Figure 9. Damage development on the positive edge.**

1. {$M \approx 39\%$ of M_{fp}} The 90° ply (plate interface ply) cracks near the step, usually at values of x between 1 and $1\frac{1}{2}t$, where t is the ply thickness (Figure 10a).

* The moment loading has been chosen here because it was felt to have a greater influence on the damage development than the tensile or shear loadings. Because of the cantilever beam apparatus and the long, thin specimens used in this testing, the bending has a much larger contribution to the tensile stress in the outer plies than the tensile loading does.

** The crack spacing on the plate face is arbitrary in the figure. In actuality the cracks are spaced much farther apart. Although the observed crack concentration does increase as the bending moment increases, there is not a clear characteristic spacing at a given load level as may be expected from simple calculations of the stresses that are due to bending.

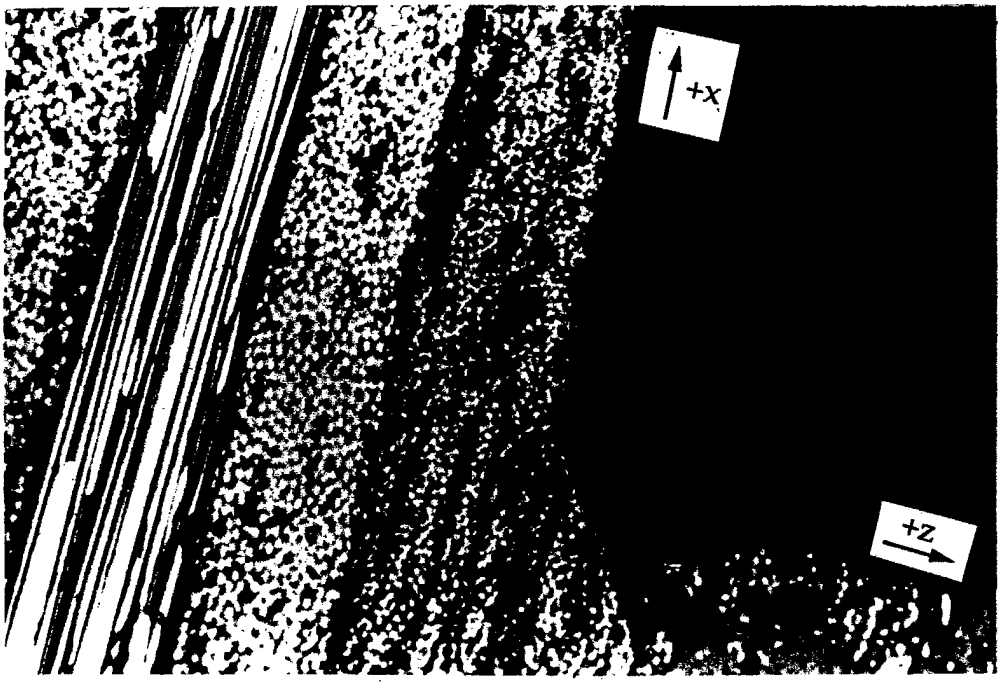

Figure 10a.[en] First crack to appear on the positive edge.

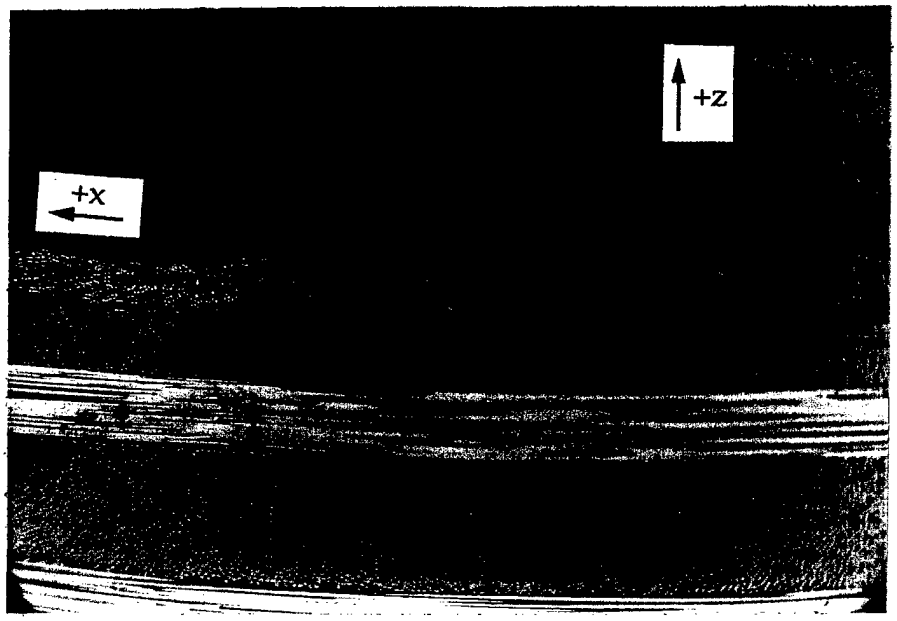

Figure 10b.[en] Additional cracking in the plate interface ply.

[en] Denotes that the photograph has been enhanced to provide better reproducibility.

2. {$M \approx 53\%$ of M_{fp}} More cracking in the 90° ply develops further away from the step at larger values of x (Figure 10b).

3. {$M \approx 73\%$ of M_{fp}} New cracks form away from the step; these cracks immediately cross both the 90° and 45° plies (Figure 10c). All 45° ply cracks which appear on the positive edge have x positions greater than or equal to those of the corresponding cracks in the 90° ply. Therefore, when viewing an area of the specimen which contains a crack crossing both plies, one usually sees the crack jog away from the step as it passes from the 90° ply to the 45° ply.

4. {$M \approx 74\%$ of M_{fp}} Several of the cracks away from the step which had only crossed the 90° ply at the lower loads now propagate across the 45° ply (Figure 10d).

5. {$M \approx 91\%$ of M_{fp}} The corner crack (crack through the 90° ply nearest the step) next extends through the 45° ply (Figures 10e and 10f).† Before the corner crack crosses the 45° ply, the largest cracks are found away from the step (in the $+x$ direction). However, shortly afterwards the corner crack appears to be the most severe crack.

6. {$M \approx 95\%$ of M_{fp}} The first few 0° fibers fracture in several places near the area where the corner crack runs into the 0° ply (Figure 10g). Also in this figure, notice the increase in mode III crack displacement over the previous figure. This increase was preceded by a large amount of noise emitted from the specimen.

---

† For the photomicrographs shown in the figures, this step actually required two load increments since the crack in the 45° ply was arrested by the resin-rich region.

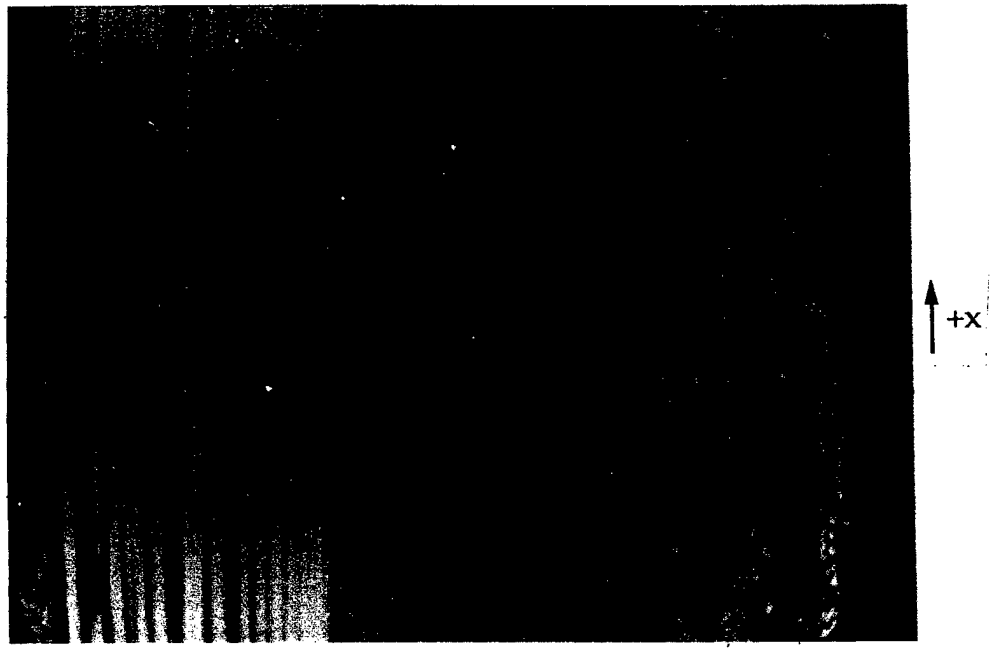

Figure 10c. Crack across the 90° plate interface ply and the 45° ply.

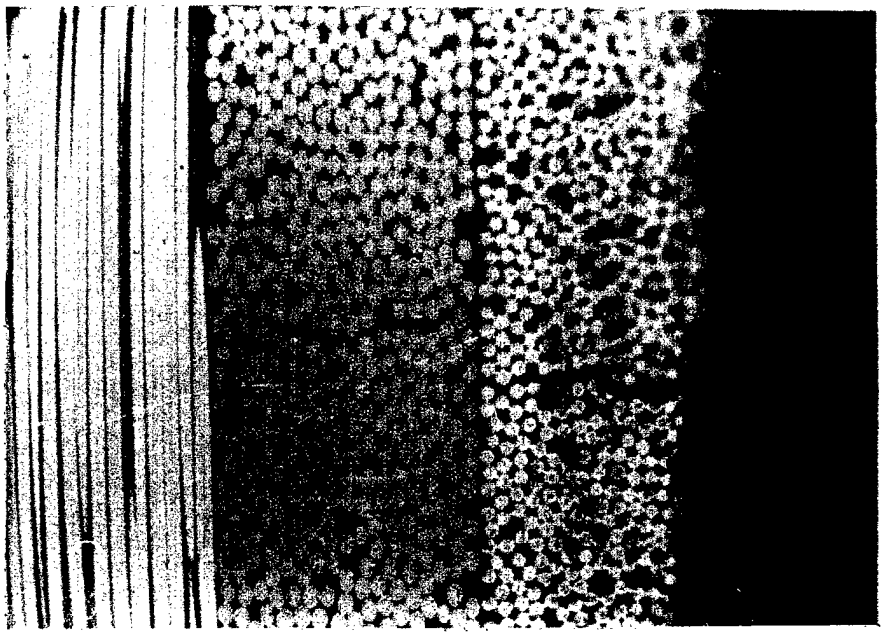

Figure 10d. Crack across the 90° plate interface ply and the 45° ply.

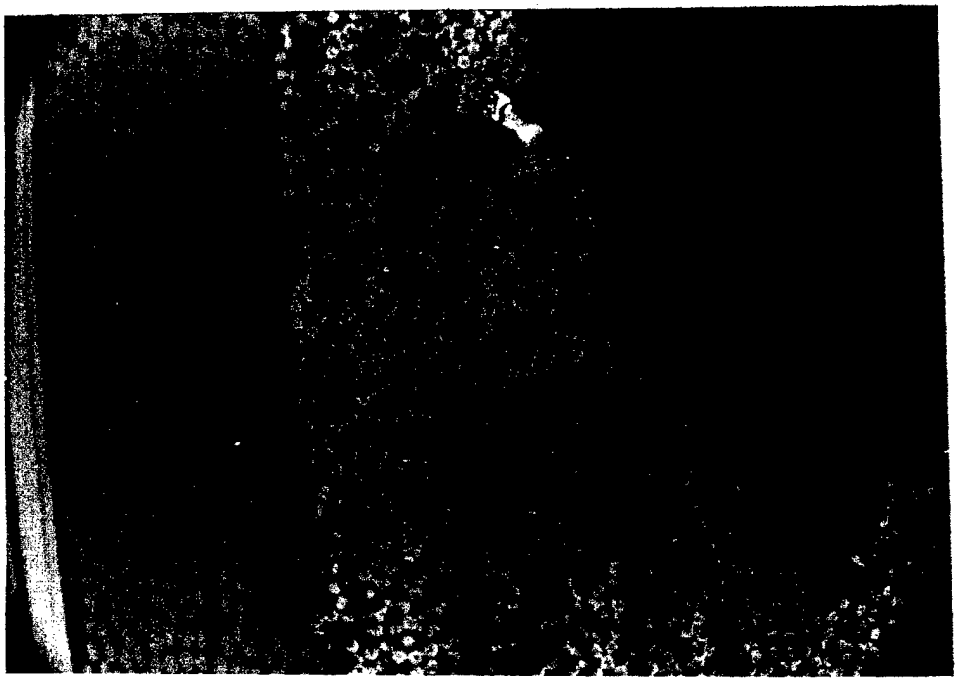

Figure 10e. Extension of the corner crack into the 45° ply.

Figure 10f. Extension of the corner crack across the 45° ply.

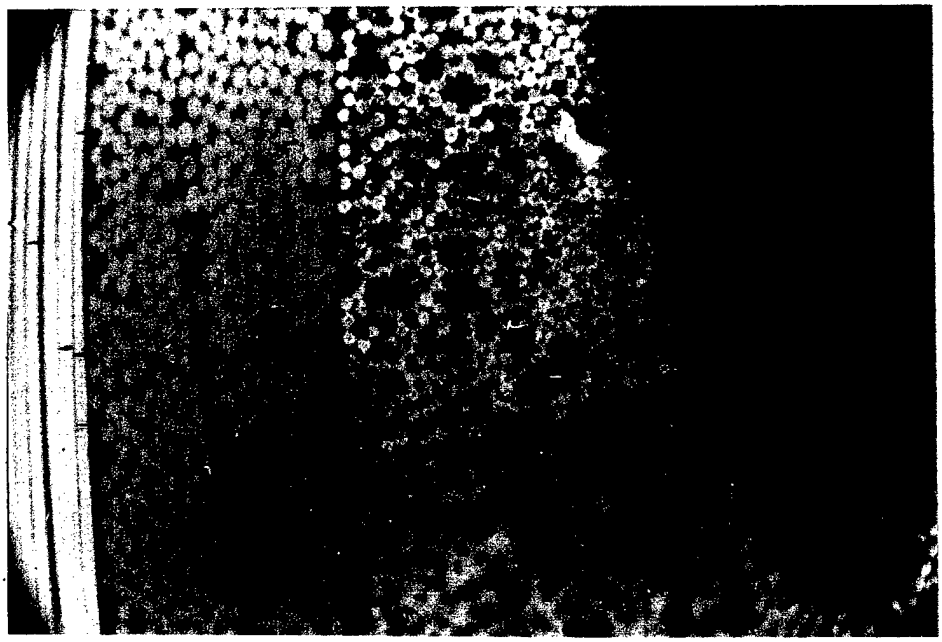

Figure 10g.[en] 0° fiber fractures and increased "mode III" displacement.

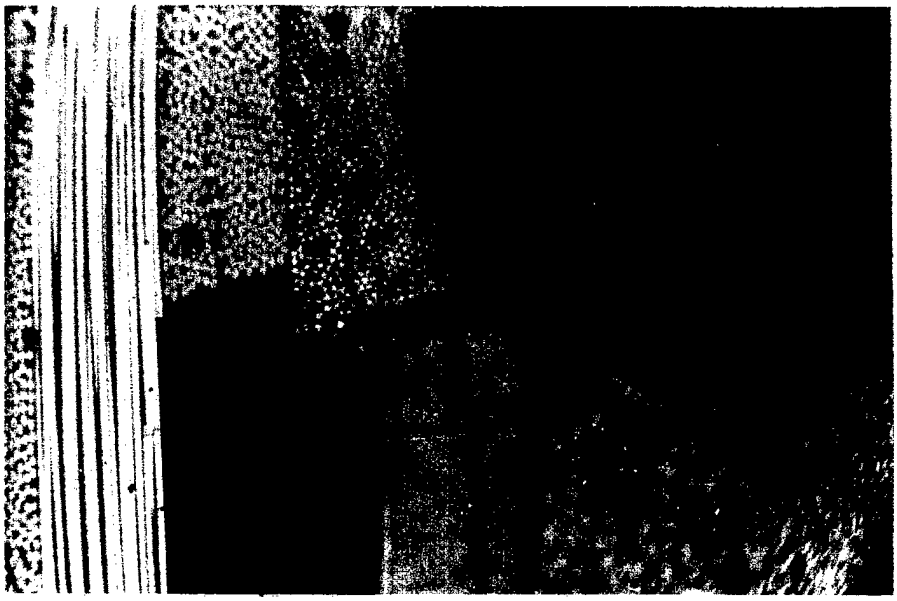

Figure 10h. Failed specimen.

7. $\{M = M_{fp}\}$ As the load increases further, the corner crack turns and propagates along the 45/0 interface into the thicker portion of the specimen, leading to catastrophic failure. As this delamination crack propagates down the interface in the $-x$ direction, it usually moves over into the 0° ply and peels that ply apart as it continues propagating toward the end of the specimen (Figure 10h).

It should be pointed out that in all of the transverse matrix cracking† observed for each lay-up, there was a clear preference for the cracks to propagate on the fiber/matrix interface as they grew across a ply (see, for example, Figure 10d). This indicates that the fracture toughness of the interface is lower than that of the matrix.

4.1.2. Observations on the Negative Edge

As on the positive edge, the location of each step in the damage process is marked in Figure 11. Here again we follow the load increase in delineating the damage development:

† Transverse matrix cracks propagate through the thickness of a ply and are oriented parallel to the fiber direction.

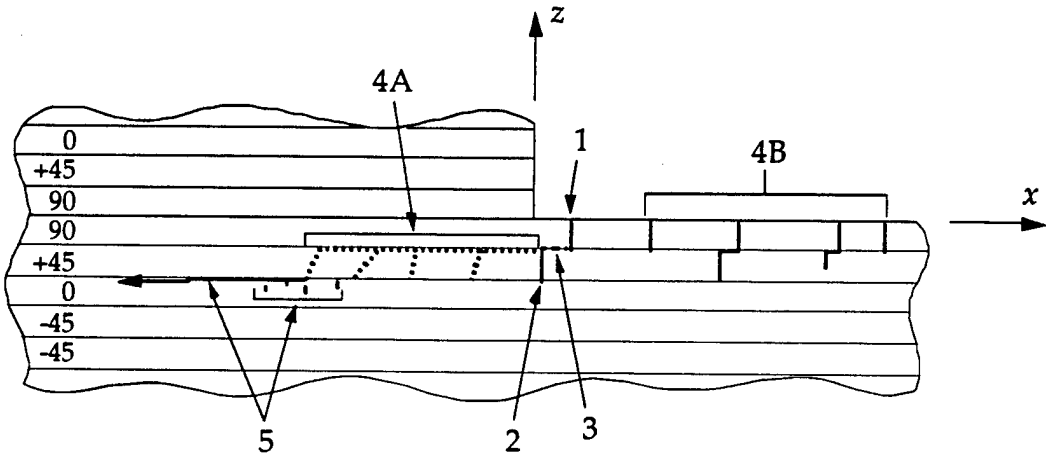

Figure 11. Damage development on the negative edge.

1. {$M \approx 41\%$ of M_{fn}, where M_{fn} is the moment loading at ultimate failure for this specimen} The first damage seen on the negative edge is also the cracking of the 90° ply near the step (Figure 12a).†† This crack, and the others which later develop in the 90° ply, cross the entire width of the specimen.*

2. {$M \approx 44\%$ of M_{fn}} The 45° ply then cracks near this fracture in the 90° ply. Each 45° ply crack which forms on the negative edge has an x position less than or equal to that of the corresponding crack in the 90° ply, just the opposite of what was observed on the positive edge (Figure 12b).

3. {$M \approx 44\%$ of M_{fn}} Immediately after the 45° ply fractures near the corner, the interface separates between the two cracks, leaving one crack on the surface, which crosses the 90° ply, jogs along the interface, and then crosses the 45° ply.

†† The damage shown in this photomicrograph actually occurred during fabrication, but it is still an accurate representation of a typical first crack generated during the test.

* This was verified by measuring the crack spacing on both edges and by performing post-mortem penetrant dye inspection of the plate face.

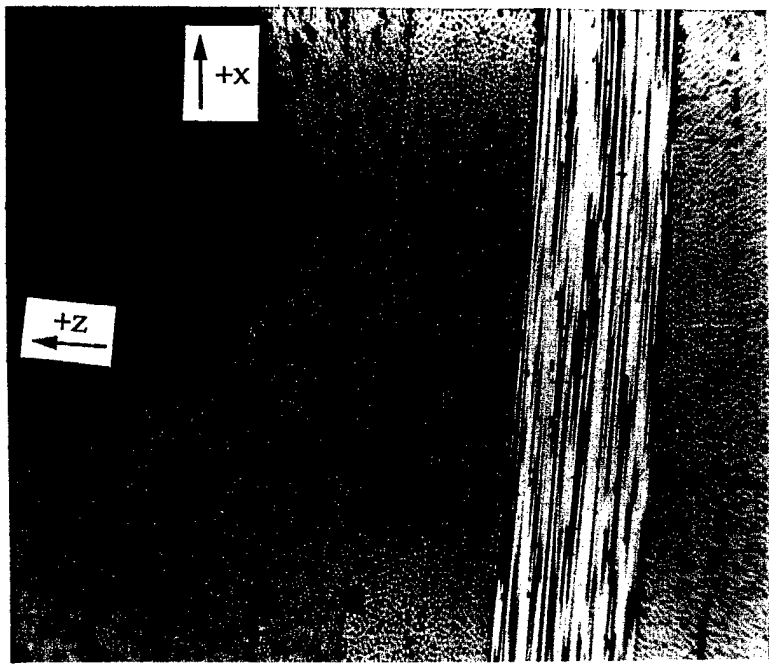

Figure 12a. First crack to appear on the negative edge.

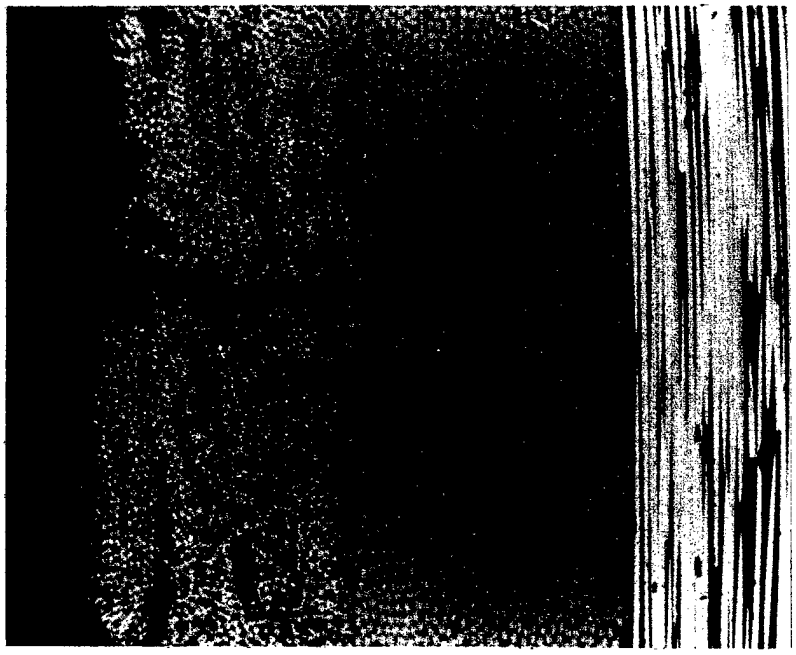

Figure 12b.[en] Cracking in the 45° ply.

4. {$M \approx 56\% - 96\%$ of M_{fn}} Next, a series of repeating steps occurs which allow the delamination to propagate in the -x direction by stable increments. The load angle, φ, is increased at each increment so that the damage process can continue. However, each one of these increments is a different size since there is not one particular stage of the process at which the crack arrests each time. In fact, it is not uncommon for the following sequence of events to be repeated several times at the same load level as the damage gets farther away from the step:

   (i) This process usually begins with the interface crack propagating farther away from the step and then turning into the 45° ply. However, sometimes the crack in the 45° ply appears before the extension of the interface crack, as shown by the crack near the bottom of Figure 12c. In Figure 12d, the same interface crack propagated farther along the specimen before turning into the 45° ply.

   (ii) Next, the 45° ply crack farthest from the step grows almost all the way across the ply. Then the delamination crack (interface crack) grows along the interface, and turns into the 45° ply again. This process is repeated several times as the load is increased (Figure 12e, "4A" in Figure 11).

As this delamination process starts to occur, additional cracking begins to develop on the plate edge on the other side of the step where x is greater than zero ("4B" in Figure 11). Some of these new cracks cross both the 90° and 45° plies, but the damage by the corner appears the most severe throughout the entire test when viewing the negative edge.

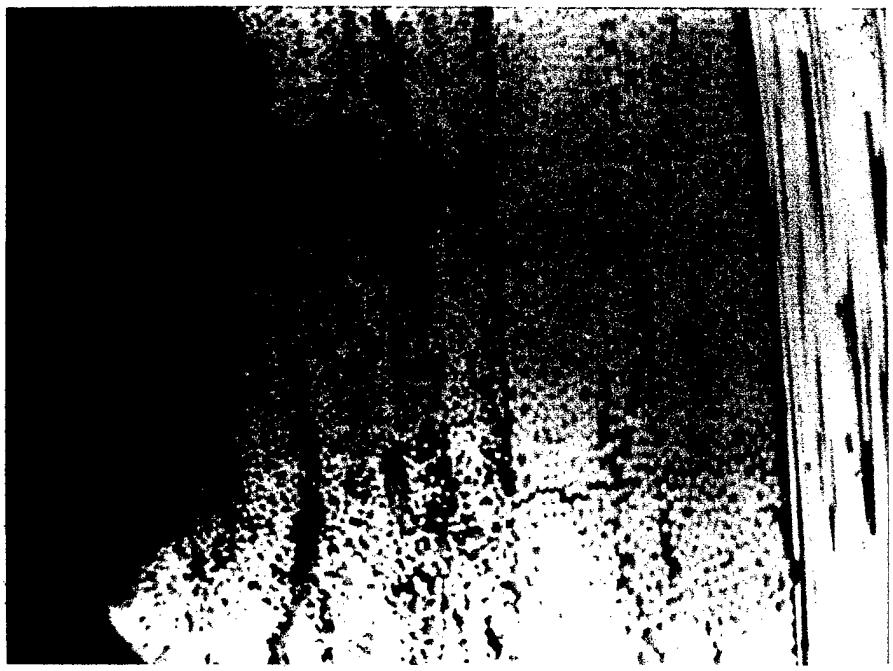

Figure 12c. The early stages of delamination propagation.

Figure 12d.[en] Continued delamination propagation.

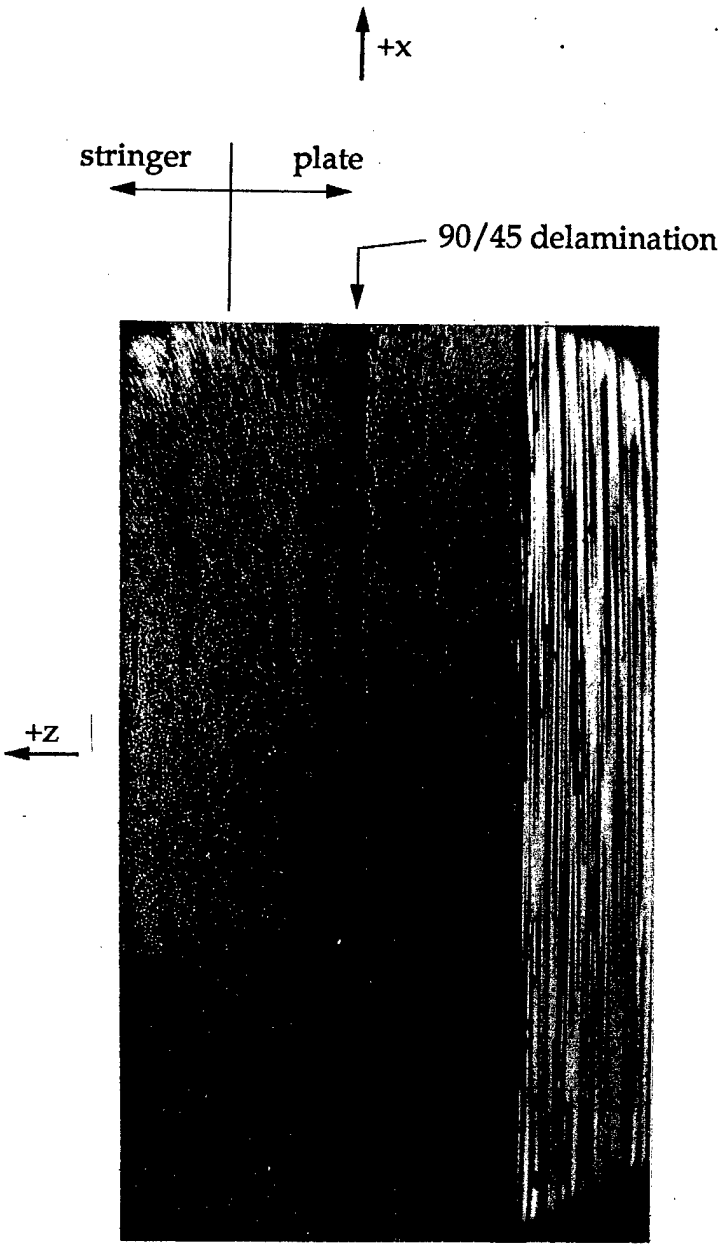

Figure 12e.[en] Continued delamination propagation.

5. $\{M = M_{fn}\}$ Finally, after crossing the 45° ply, the crack with the most negative value of x turns and propagates along the 45/0 interface. As seen on the positive edge, the area where the crack starts to propagate on this interface usually contains several broken 0° fibers. At this point the crack propagation is usually unstable and leads to catastrophic failure. Again, as noted in the observations on the positive edge, this crack often moves from the interface to within the 0° ply as it runs toward the end of the specimen (Figures 12f and 12g).

4.1.3. Overall Damage Process

This section suggests mechanisms in an attempt to describe the damage development in the specimen. Since several of these mechanisms relate to events that could not be directly observed in the tests, much of the following discussion represents the writer's best hypothesis of the mechanisms involved.

As mentioned earlier, the damage process begins with cracking in the 90° ply near the step. There are two very interesting observations that can be made from this initial damage:

(i) The crack usually does not occur right at the corner, where on the basis of linearized (homogenized lamina) analysis, one would expect a singularity, or at least the highest stresses.

(ii) The presence of the step does not seem to affect the crack angle, α, as defined in Figure 13. For this lay-up the matrix cracks almost always

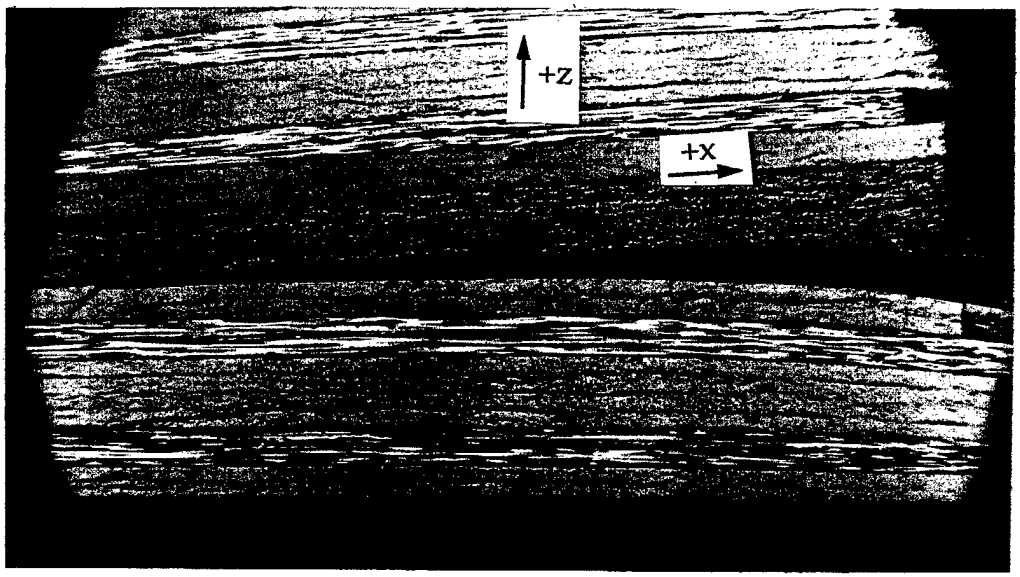

Figure 12f. Failed specimen.

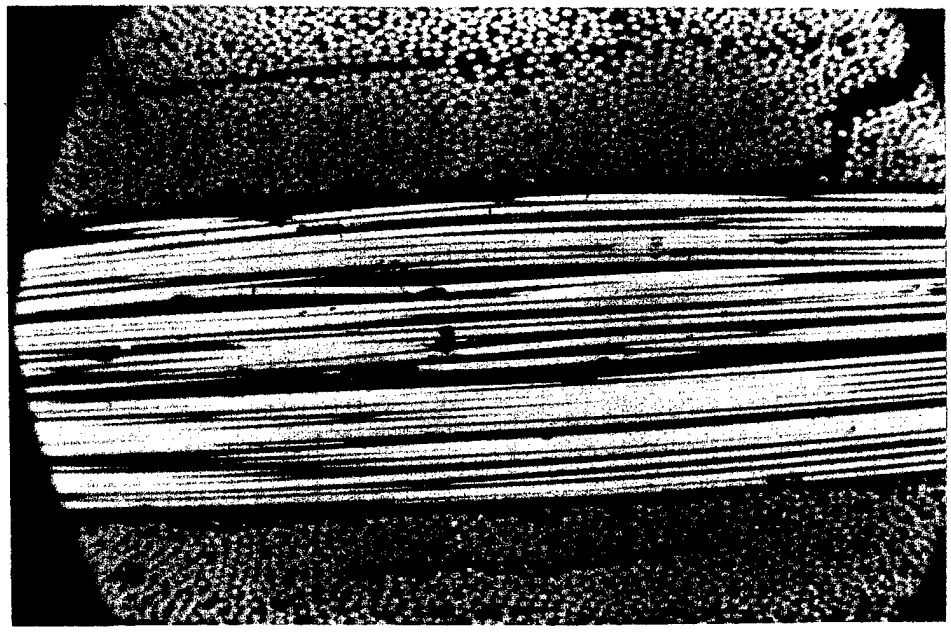

Figure 12g. Close-up of the region near the left of Figure 12f, where 45/0 delamination began.

run straight across the plies, regardless of how close they are to the corner. This observation seems to contradict the numerical, asymptotic solution by Kubr, which would indicate that the lines of principal stress in the plate interface ply directly below the step (-z direction) are 45° different from the lines of principal stress in the same ply out away from the step (+x direction) (Figure 13).

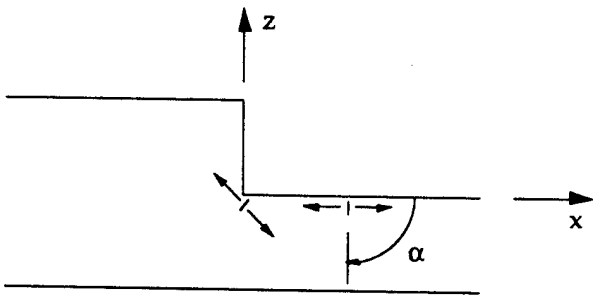

Figure 13. Directions of maximum normal stress calculated from the results of Kubr's numerical study.

These two features indicate that the failure process is not entirely driven by the nature of the "analytical stress singularity," as may be widely believed. It is true that failure does initiate *near* the corner, but since it is not right *at* the corner, one can deduce that the precise structure of the geometry and of the singularity does not completely govern failure initiation. It seems that for composite materials, the local variation in material parameters, combined with the inherent ability of composites to redistribute loads away from regions of high stress, often prevents the singularity from dominating the failure mechanism. This suggests that in modeling a stepped composite plate, it may not be wise to spend a lot of resources on developing a precise

description of the singularity within an extremely small vicinity of the corner.†

After the 90° ply cracks near the step, more load is redistributed to the 45° ply in that area. Because of the stress singularity at the crack tip, one might expect the 45° ply to begin cracking near the 90° ply crack when the load gets high enough. This cracking would be distributed throughout the width of the plate if one did not have to account for free-edge effects. However, since simple beam-type specimens were used in this work, the free edges did influence the damage development. Therefore, the stresses will be higher near the edges.

One other effect which contributes to the location of maximum stress is the twisting of the specimen. This effect is mainly caused by the 45° plies near the surface of the plate, as shown in Figure 14. For a given axial stress, there is a larger strain transverse to the fibers than parallel to them. This skews the axis about which the specimen bends, giving a smaller radius of curvature, and therefore a higher bending stress, along the negative edge.

† The above comments do not imply that a stress concentration does not exist on the 90/90 interface at the corner. It just turns out that for this lay-up, the matrix normal stress (in-plane tensile stress perpendicular to the fibers) in the 90° plate interface ply reaches a critical value before the opening stress on the interface does.

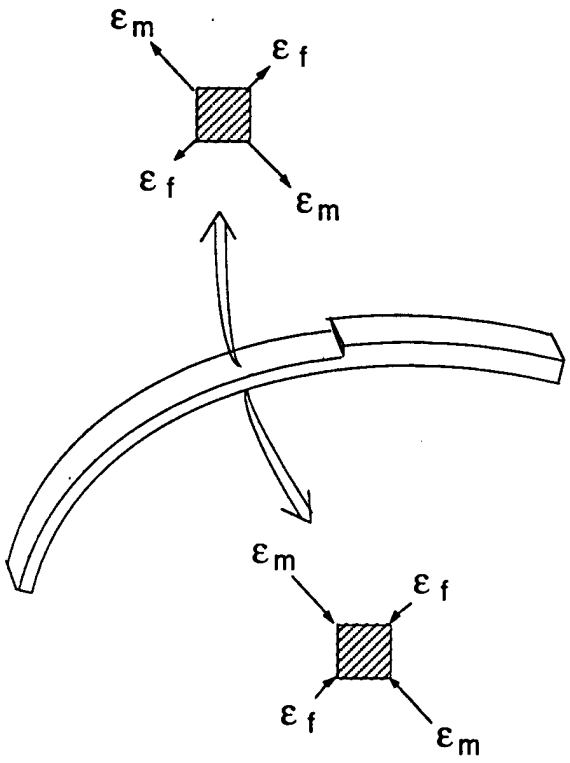

Figure 14. Specimen twist mechanism.

The intersection of the high-stress regions caused by all of the above mechanisms is in a small area near the tip of the 90° ply crack within one ply thickness of the negative edge. Therefore, when the load becomes high enough, the next type of damage to appear is cracking in the 45° ply in this region. Because of the variation in parameters such as fiber position and fiber volume fraction, the area where the stresses first exceed the fracture level is not always right *at* the negative edge. If this area happens to be just inside the specimen, then the matrix crack in the 45° ply intersects the edge at an x position slightly less than that of the 90° ply crack. This observation explains why many of the cracks viewed on the negative edge jogged toward the step as they travelled from the 90° ply to the 45° ply (Figure 11). Similarly, when

matrix cracks in the 90° and 45° plies intersect near the positive edge, the cracks viewed on the surface often jogged away from the step (in the $+x$ direction) (Figure 9).

When a crack in the 45° ply forms near the end of the step by the negative edge, a triangular region of the interface is isolated (Figure 15a), causing it to be loaded with a very high shear stress. This is most easily seen by considering a force-balance diagram of the cracked portion of the specimen near the negative edge (Figure 15b):

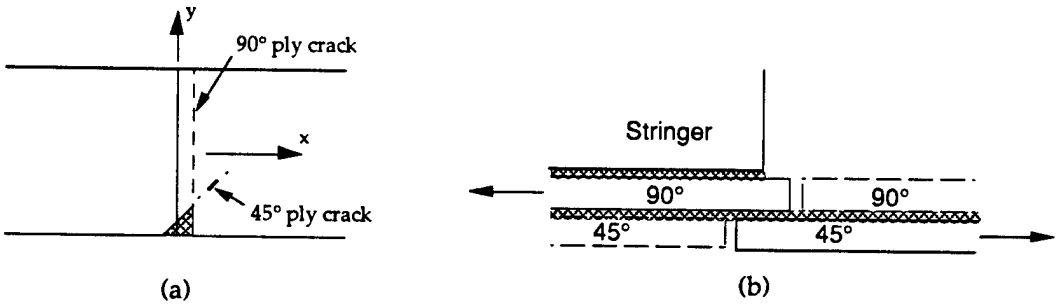

Figure 15. Region of high shear stress.
(a) plan view (b) negative-edge view.

The plies are under a tensile loading away from the crack because of the bending. Since both the 90° and 45° plies are unable to support a tensile stress near the transverse cracks, the entire force is transferred through the small overlapping region of the interface. This makes the shear stress in this area very high, causing the interface to fracture. Therefore, for this lay-up, the damage development indicates that delamination initiation is caused by interlaminar shear stress.* Although this feature appears to be a direct result

* This agrees with some numerical and experimental work on tension-compression fatigue of composites by Ratwani and Kan [1982], in which they also found interlaminar shear stresses to be a more likely source of delamination than interlaminar normal stresses.

of the finite-width specimen geometry, it is believed that the same mechanism would be found in very wide plates, as will be discussed later.

The hypothesis that the delamination initiates on the negative edge has been substantiated by performing ultrasonic C-scans on two specimens, one of lay-up case 1 and one of case 2, shortly after delamination was detected on the negative edge. Since neither of the C-scans could resolve this damage, it could be concluded that the delamination was localized to the edge, and that the observations on the negative edge were not indications of a larger delamination in the interior of the specimen.

The above discussion on delamination initiation for lay-up case 1 has focused on finite-width specimens, where the free edge provides one of the borders for the region of high shear stress shown in Figure 15. However, one must realize that the same mechanisms also apply to wide plates, e.g., stringer-reinforced skin panels. In situations where free-edge effects are not important, the delamination will still start by one of the areas where the 45° and 90° ply cracks cross. This is so because the tensile stress in the plies is approximately constant across the width of the specimen (neglecting twist), and the area per unit width in which the tensile stress can be transferred from one ply to the other is smallest near the crack intersection, causing the shear stress to be highest there.

At this stage in the damage process, there is a crack through the 90° ply near the step, a small triangular section of the interface, which is delaminated, and a crack across the 45° ply at the $-x$ end of this interface crack. The next type of damage to appear is the propagation of the delamination

along the interface in the -x direction. There are two mechanisms which contribute to the high peel stress responsible for delamination propagation:

(i) As seen in Figure 16, the beam shear force, V, gives a mode I opening stress on the delamination crack.

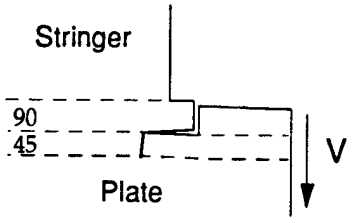

Figure 16. The effect of beam shear force on delamination.

(ii) The discontinuity in bending stiffness also contributes to this opening stress since the plate tends to deflect much more easily than the plate–stringer combination (Figure 17).

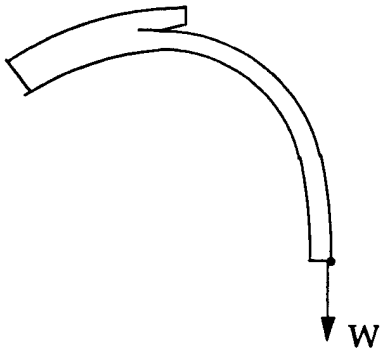

Figure 17. Delamination caused by different bending stiffnesses.

One difficulty in partially attributing the delamination propagation to beam shear force is that in a two-dimensional drawing, this seems to be an unstable process. Figure 18 implies that as the delamination crack tip moves in the -x direction, the shear force at the crack tip increases if the load angle, φ, is less than 90°. This apparent instability seems to contradict the negative-

edge observations, which indicated that the early stages of delamination were a stable process.

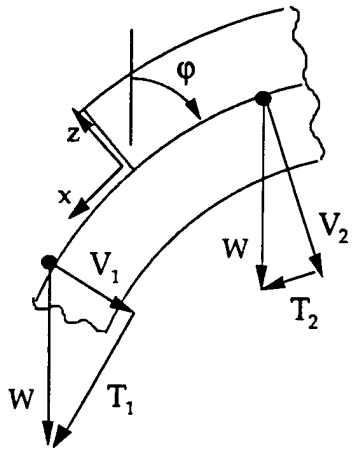

Figure 18. The relation of beam shear force to delamination tip position.

However, when viewing the delamination crack front in plan view (Figure 19), one realizes that the amount of new surface area per unit crack advance increases as the delamination grows across the specimen. In terms of the Griffith criterion for crack advance, this increases the total energy required for each subsequent unit of crack propagation. Therefore, since the required energy is increasing as the shear force is increasing, it is no longer clear whether the process is unstable.

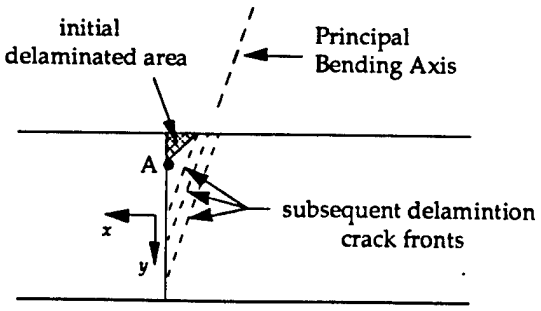

Figure 19. Plan view of delamination crack advance.

The above discussion has shown that the high peel stress caused by the beam shear force and the discontinuous change in bending stiffness can provide a stable means of driving the delamination crack forward. However, there are some other features about the delamination process that warrant further discussion. The crack-front propagation form shown in Figure 19 has been deduced by the author's interpretation of the C-scans shown in Figure 20.

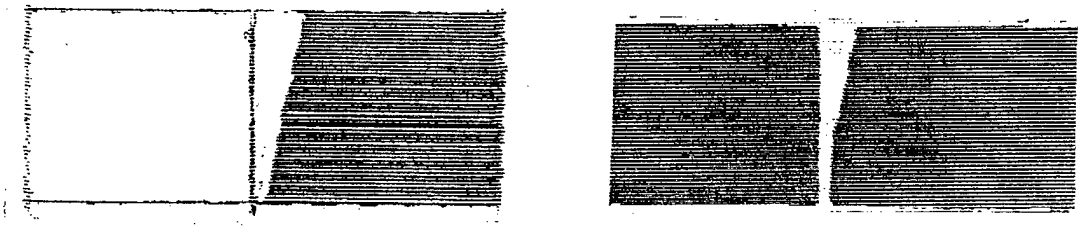

(a) (b)

Figure 20. C-scans of partially delaminated specimens.*
(a) Lay-up case 1. (b) Lay-up case 2.

Even though the C-scans are for two specimens of different lay-ups, it is believed that the delamination crack front is parallel to the axis about which the specimen is bent in both cases. This axis will be referred to as the principal bending axis in the following discussion. Because of the bending-twisting coupling introduced by the ±45° plies (Figure 14), the axis does not cross the specimen at 90°. This deviation is believed to cause the plate side of the specimen to peel away from the stringer asymmetrically. In the appendix, the orientation of the principal bending axis for the case 1 specimens has been calculated. It turns out that it coincides quite well with the delamination

* The two C-scans appear differently because one (case 1) was performed as an impulse-echo test, while the other (case 2) was performed as a through-transmission test.

crack front, giving support to the above hypothesis. Therefore, the crack-front propagation is described in the following manner:

(i) After the initial 45° triangular delamination crack forms, the highest stress is at point A in Figure 19.

(ii) The part of the crack front by point A then propagates until the crack front is parallel to the principal bending axis.

(iii) The crack front then advances uniformly until it reaches the positive edge of the specimen.

Another part of the delamination mechanism that should be explained is its relation to transverse matrix cracking in the 45° ply, as observed on the $-x$ portion of the negative edge (Figure 21).

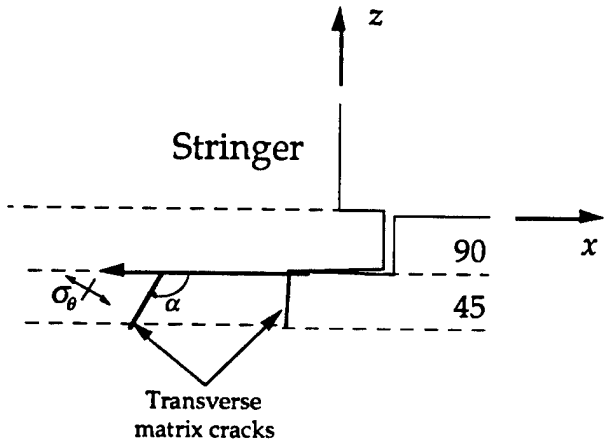

Figure 21. Cracking in the 45° ply on the $-x$ side of the step.

Referring to Figure 21, after the delamination crack travels along the interface, away from the previous crack in the 45° ply, the tensile stress below the crack tip increases. This causes the circumferential stress at the delamination tip, σ_θ, to increase in directions below the interface. When σ_θ in some direction below the interface is significantly larger than σ_θ on the

interface, the crack kinks into the 45° ply.* When the crack impinges on the 0° ply, the composite's resistance to fracture, e.g., $\sigma_\theta|_{crit}$, becomes much larger, causing the crack to arrest. Now that there is a free surface crossing the 45° ply by the delamination crack tip, the ratio S (defined in the footnote) is maximum along the interface. Therefore, when the load is high enough, the crack propagates along the interface, and the process repeats.

It should be pointed out that this explanation can be modified to account for the occasions when the delamination crack resumes its propagation along the interface before the crack in the 45° ply reaches the 0° ply. In order to understand this situation, the reader must again be reminded of the three-dimensional shape of the delamination crack. Since the crack front lines up with the principal bending axis and not with the 45° fibers, the apparent kinking of the delamination crack as seen from the negative edge leaves most of the delamination crack front unchanged (Figure 22):

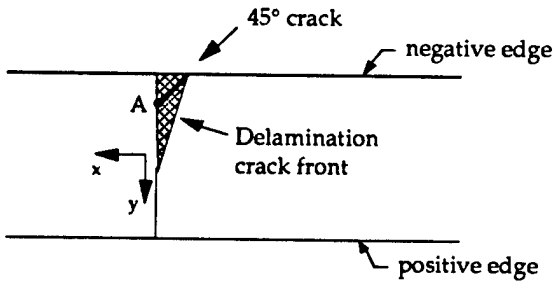

Figure 22. Plan view of delaminated area.

* The angle and local loading required to kink the crack can be more precisely defined in terms of the ratio $S \equiv \frac{\sigma_\theta}{\sigma_\theta|_{crit}}$. When S for some direction below the interface becomes larger than S on the interface (and larger than 1), the crack kinks in the direction of S_{max}. As shown in Figure 21, the angle, α, at which the crack crosses the 45° ply in the region on the $-x$ side of the step is not always 90°, as it was on the $+x$ side.

When the delamination crack bends into the 45° ply (as seen from the negative edge), some of the load that was carried near the negative edge is redistributed to the interior of the specimen. This increases the opening stress of the interface crack inside the specimen, and causes the delamination front to advance. As discussed earlier, the delamination is believed to advance uniformly. Therefore, the crack is seen to start propagating along the interface again when viewing the negative edge.

The above explanation for the kinking of the interface crack is also supported by the orientation and position of the cracks in the 45° ply. As the delamination grows in the $-x$ direction, cracks in the 45° ply which occur a larger distance beyond the previous 45° ply crack tend to cross the ply at a crack angle, α, closer to 90°. For example, in Figure 21, if the distance between the two transverse matrix cracks in the 45° ply is large, then it is likely that the second crack (the one on the left) will be oriented at a crack angle closer to 90°. However, if the distance between the two cracks is small, then α is likely to be closer to 180°. This fracture behavior is reasonable since the tensile stress that is due to bending is higher in areas farther from the 45° ply cracks.† This fact maximizes σ_θ at a smaller angle (closer to 90°) when the delamination crack tip is in one of these areas of higher bending stress.

As the delamination propagation just described begins, more damage starts to develop also on the $+x$ side of the plate face away from the step. This damage is the result of the increased tensile stress on the plate face that is due to the larger load angle. The first cracks to appear pass through the 90° ply

† At the crack locations, the tensile stress that is due to bending is zero because of the traction-free crack surfaces.

and cross the entire width of the specimen. Then as more load is transferred to the 45° ply, it too develops transverse matrix cracks. However, the progression of cracking in the 45° ply can be difficult to explain, especially when viewing the positive edge. The first cracking in the 45° ply on this edge is located well away from the corner. Since the moment arm, *d* (Figure 6), at the corner is larger than the moment arm anywhere else on the plate, this seems to imply that the first cracks don't appear where the tensile stress is highest. However, it is believed that these cracks actually originate in the interior of the specimen near the step. As mentioned previously, the specimen twist causes the first cracks in the 45° ply to form near the intersection of the step and the negative edge. As the load increases, more cracks develop closer to the positive edge, and the existing cracks propagate on a 45° angle (plan view) away from the step. Therefore, the first cracks to reach the positive edge do not usually intersect it near the step.*

When a crack reaches the positive edge, the stress singularity by the crack, combined with the free-edge singularity, causes the 90° ply to immediately fracture near the intersection of the 45° ply crack and the edge. This behavior explains why the 45° ply was never seen to fracture before the 90° ply. As mentioned earlier the cracks often intersect slightly away from the free edge, causing the crack on the edge to jog away from the step as it passes from the 90° ply to the 45° ply.

---

* This hypothesis, that cracks form by the step at various points across the width of the specimen, received some support in the observations of case 2 specimens, which have a 45° plate interface ply, and will be discussed later. At this point it suffices to say that cracking in the 45° ply of the case 2 specimens was clearly distributed throughout the width of the plate interface ply by the step.

The next damage to occur on the positive edge is the propagation of the cracks that had previously crossed only the 90° ply. When the stress in front of these cracks gets high enough (this occurs near the free edge), they advance across the 45° ply. However, the first cracks to propagate across the 45° ply are located away from the step. This part of the damage process is the most difficult to explain. Since this new cracking is clearly an extension of the previous damage in the 90° ply, it cannot be explained as originating inside the specimen near the step as before. Therefore, it again appears as if damage is initiating in an area where the bending stress is not highest. A simple explanation for this inconsistency has not been found. However, it should be pointed out that the state of stress is very complicated at this stage in the damage process since the changes in geometry that are due to cracking have altered the stress field. The tensile stress in the 45° ply caused by bending is not simply proportional to the length of the moment arm. The higher concentration of cracks in both plies away from the step makes the effective load-carrying thickness of the specimen thinner in that region, thus lowering the moment of inertia and raising the stress. Although the additional cracking in the 90° ply will tend to raise the stress in the 45° ply in that area, the 45° ply will be relieved of some stress when it develops cracks. The net effect of these mechanisms is not readily determined.

When the local loading by the intersection of the corner crack and the positive edge reaches a critical value, this crack, too, extends across the 45° ply. After the load is raised slightly higher, a substantial increase in mode III displacement of the crack is observed. The perceived mode III displacement is

the y component of the 45° ply crack-opening displacement, which is believed to have two sources (Figure 23):

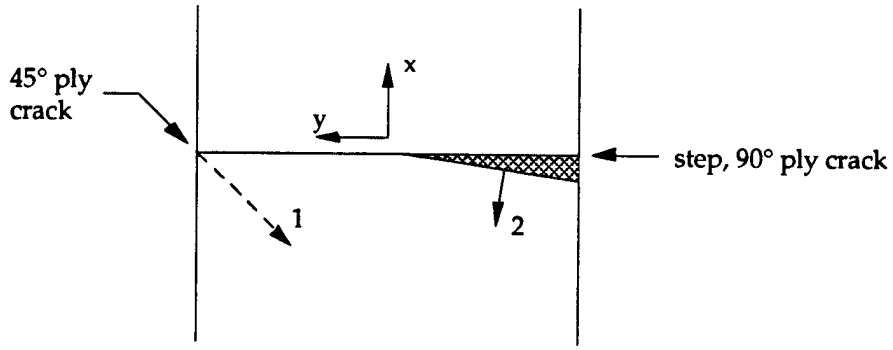

Figure 23. Contributions to "mode III" displacement.

First, as the crack in the 45° ply propagates into the specimen, the crack-opening displacement at the free edge increases. Second, as the 90/45 delamination spreads across the specimen, the curvature of the 45° ply increases as the portion of the plate below the delamination (-z direction) peels away from the stringer and 90° ply above the delamination. This increase in curvature causes the tensile stress in the 45° ply to increase ahead of the delamination tip as well as behind it, thus increasing the opening stress and crack-opening displacement of the 45° ply crack near the corner. This second contribution is believed to be the cause of the damage noise which preceded the perceived mode III displacement.

Because of the 90/45 delamination and the additional cracking of the 45° ply, the bending stiffness of the plate decreases as one travels in the -x direction within the damaged area of the specimen. This means that the specimen curvature, and therefore the crack-opening stress, is now highest by the crack in the 45° ply with the lowest value of x. This crack is the last transverse matrix crack to occur in the 45° ply by the negative edge and

extends from the 90/45 delamination tip to the 0° ply. As the load is increased, some of the 0° fibers fracture in front of the crack. However, since the fracture toughness of the 0° ply is very high, the stress on the 45/0 interface exceeds the level required to kink the crack in the -x direction well before the load becomes high enough to break the 0° ply. The crack then moves to the 45/0 interface and usually becomes unstable, causing the specimen to fail catastrophically.

The details of the 45/0 delamination are most easily recognized by analyzing the fracture surface. In all of the case 1 and 4 specimens, the fracture surface can be represented by Figure 24.

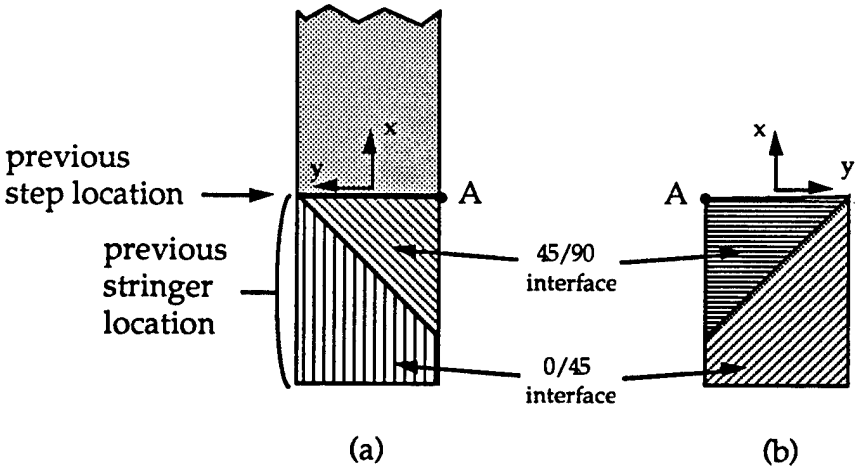

Figure 24. Fracture surface of case 1 and 4 specimens. (a) Plate side of the fracture surface. (b) Stringer side of the fracture surface.

One may wonder why the final separation crack of the 45° ply always coincides with the intersection of the step and the positive edge. After all, the 45/0 delamination often begins much closer to point A.* This difference is best understood by considering the alternatives to the fracture surface of

* On the negative edge it began at values of x between $-\frac{1}{16}$ and $-\frac{1}{4}$ inch.

Figure 24. Since the local loading increases as one travels toward the y axis from the $+x$ side, it is clear that the final separation crack in the 90° ply will be located by the step. Therefore, we need only consider the alternative positions of the 45° ply separation, as shown in Figure 25:

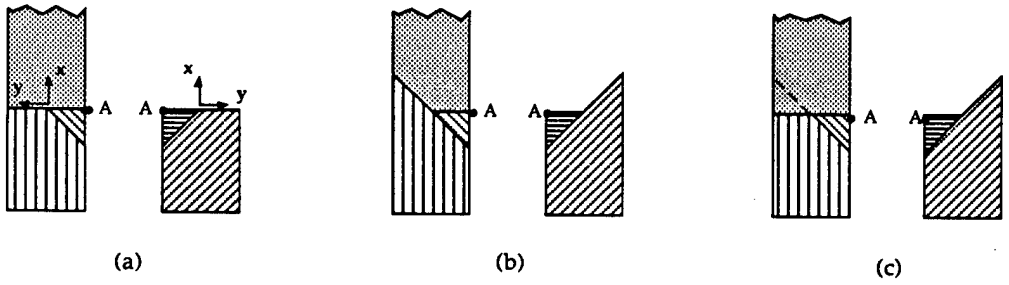

Figure 25. Alternative fracture surfaces.

The 90° plate interface ply prevents the 45° ply below it from separating freely at values of x greater than that for the 90° crack. One way in which the 45° ply can peel away from the plate differently than shown in Figure 24 is if some of the fibers break where they cross the 90° ply crack (Figure 25a). Another method that allows this to be achieved requires the 90° fibers in the plate interface ply to break where they cross the 45° ply crack (Figure 25b). One other way is for the 90/45 and the 45/0 interfaces to delaminate by the triangular portion of the 45° ply protruding above the step (Figure 25c). This will then allow the 45° ply to be pulled out from underneath the 90° ply when it separates.

Since the first two alternative mechanisms shown in Figure 25 require large numbers of fibers to fracture and separate, it is easy to see on physical grounds why the observed fracture surface requires less energy. For the surface of Figure 24 to be created, the 90/45 delamination crack must continue

propagating all the way down to the crack in the 45° ply, which originates at the corner on the positive edge. This means that the 90/45 delamination will extend one inch in the $-x$ direction from the step on the negative edge. Since the 45/0 delamination begins on the negative edge at x values between $-\frac{1}{16}$ and $-\frac{1}{4}$ inch, there is a large area where both faces of the 45° ply are delaminated. As mentioned above, this peculiarity is caused by the presence of the 90° plate interface ply, which prevents the 45° ply from peeling away from the plate less than 1 inch below the y axis on the negative edge.

Even though the third mechanism which would allow the 45° ply to separate at positive values of x usually involves less total delamination area, it doesn't occur because the stresses are much less where x is positive. In particular, the mode I opening stress for the 90/45 interface is almost negligible on the $+x$ side of the 90° separation crack. Neither of the mechanisms which contribute to delamination propagation have a significant effect on the peel stress in this region. As illustrated in Figure 26, the existence of a significant interlaminar tensile stress caused by beam shear force requires the 90° ply to move in the opposite direction as the 45° ply does. This is not the case on the $+x$ side of the 90° separation crack.

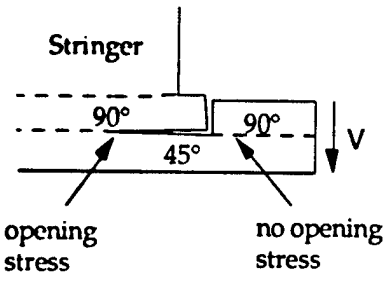

Figure 26. The contribution of beam shear force to the opening stress on the 90/45 interface.

Also, a significant opening stress in this region due to bending would require a sizable change in bending stiffness between the portion of the plate with the 90° plate interface ply and the portion without it. This also does not occur. Therefore, the stress levels needed to delaminate the 90/45 interface on the $+x$ side of the step do not exist. This makes it clear why the fracture surface consistently appeared as shown in Figure 24.

4.2. Lay-up Case 2

Similar to the previous section for lay-up cases 1 and 4, this section presents the commonly observed damage events for the case 2 specimens. Again, one specimen was selected for each edge view to represent the typical moment loadings seen at the various levels of damage development. As before, the load listed at each step is a percentage of the ultimate failure loading for the specimen.

4.2.1. Observations on the Positive Edge

As the load angle, φ, was increased during the test, the damage progressed through various stages when viewing the positive edge. Each of these stages is described below and is illustrated in Figure 27.

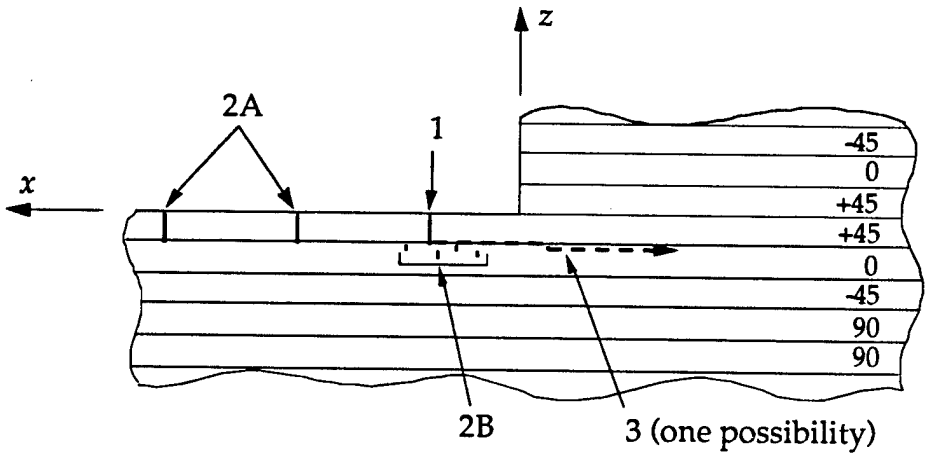

Figure 27. Damage development on the positive edge.

1. {$M \approx 77\%$ of M_{fp}} Damage is normally heard before the first crack is seen, indicating that damage does not initiate on the positive edge. However, when the first crack does reach the edge, it is usually a few ply thicknesses away from the corner (Figure 28a).

2. {$M \approx 93\%$ of M_{fp}} As the load angle increases, more cracking is seen farther away from the step at larger values of x (shown by "2A" in Figure 27). However, not nearly so many cracks develop on the edges of the case 2 specimens as did for cases 1 and 4. When viewing the positive edge of a case 2 specimen, only 2 or 3 cracks are seen before failure, compared with over a dozen cracks in the case 1 and 4 tests.

At approximately the same load, 0° fiber fractures are often observed ahead of the 45° ply crack nearest the corner (shown by "2B" in Figure 27). In some cases this crack even turns and begins to propagate stably in the -x direction along the 45/0 interface (Figure 28b).

Figure 28a. First crack to appear on the positive edge.

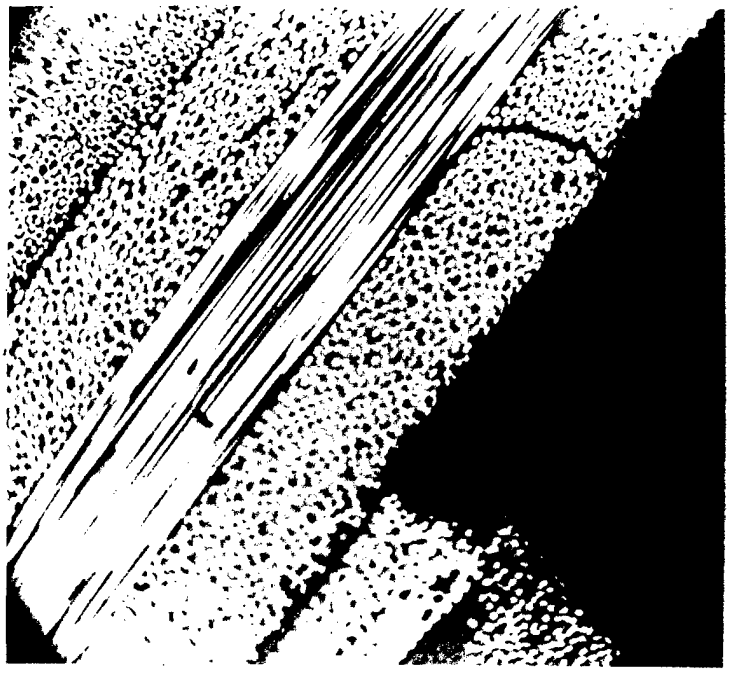

Figure 28b. Stable propagation along the 45/0 interface.

3. {$M = M_{fp}$} At this load level, the specimen fails catastrophically. However, the final fracture location is not always predictable when viewing the positive edge. For example, even though the location of the final fracture appeared to be quite obvious for the specimen shown in the previous two figures, the actual place where the specimen failed did not even contain a crack before it peeled apart (Figure 28c).

4.2.2. Observations on the Negative Edge

On the negative edge the damage progressed in the following manner:

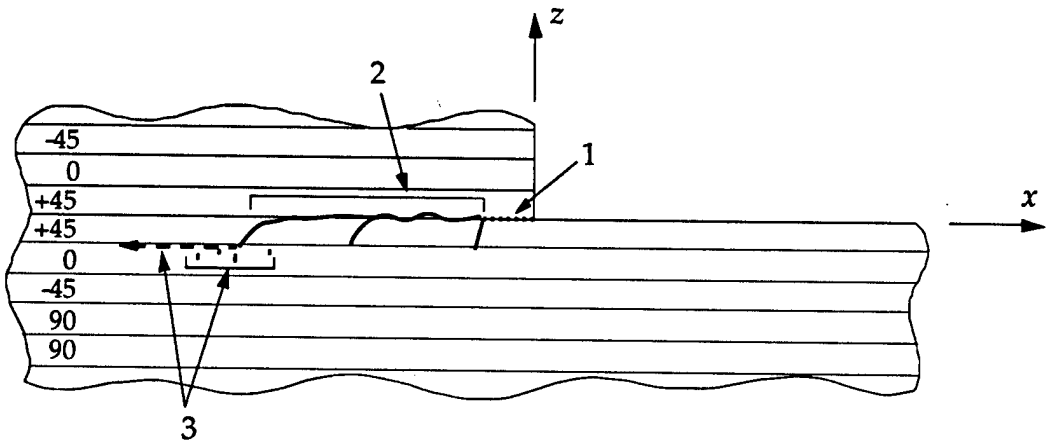

Figure 29. Damage development on the negative edge.

1. {$M \approx 70\%$ of M_{fn}} The first damage to appear on this edge is a crack on the 45/45 interface. This crack originates from the corner and travels in the $-x$ direction. Unlike case 1 and 4 tests, the delamination here does not usually occur after the appearance of a crack in the 45° ply. The significance of this

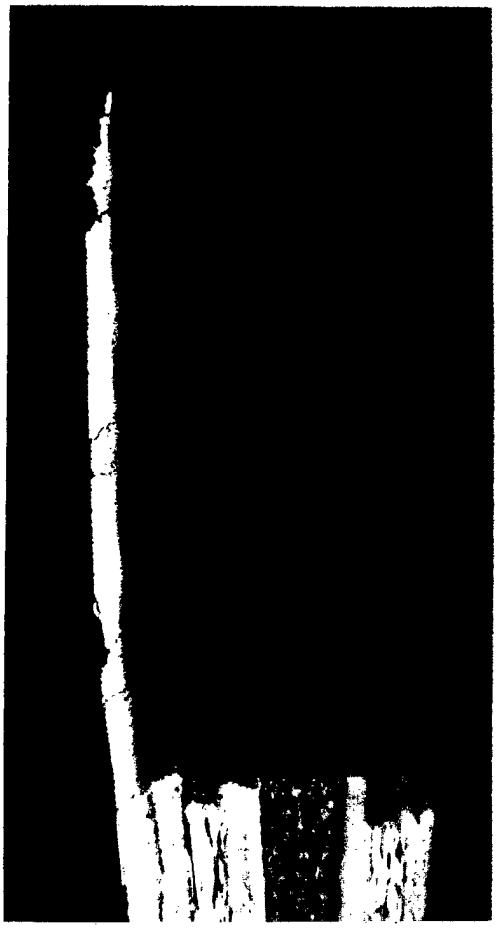

Figure 28c. Failed specimen.

point will be discussed later when delamination initiation mechanisms are considered. It should also be noted that in one of the case 2 specimens tested, a significant amount of damage noise was heard before the interface crack appeared on the negative edge. This observation indicates that damage initiation occurred in the interior of this specimen.

2. $\{M \approx 70\% - 90\% \text{ of } M_{fn}\}$ As the load increases, the delamination propagates along the 45/45 interface as discussed previously for case 1 and 4 specimens: The crack propagates along the interface, turns into the 45° plate interface ply, then resumes its propagation along the interface. As before, this process is repeated several times. However, for this lay-up there is no well-defined interface (surface) which separates as the the specimen peels apart. Instead the delamination crack tends to wander back and forth more across the 45° plies (Figure 30).

3. $\{M = M_{fn}\}$ Eventually, the delamination moves to the 45/0 interface and causes catastrophic failure. The region where this occurs often contains broken 0° fibers.

It should also be pointed out that the only damage to appear on the negative edge was that associated with the delamination. No cracking was seen at larger values of x in the plate interface ply.

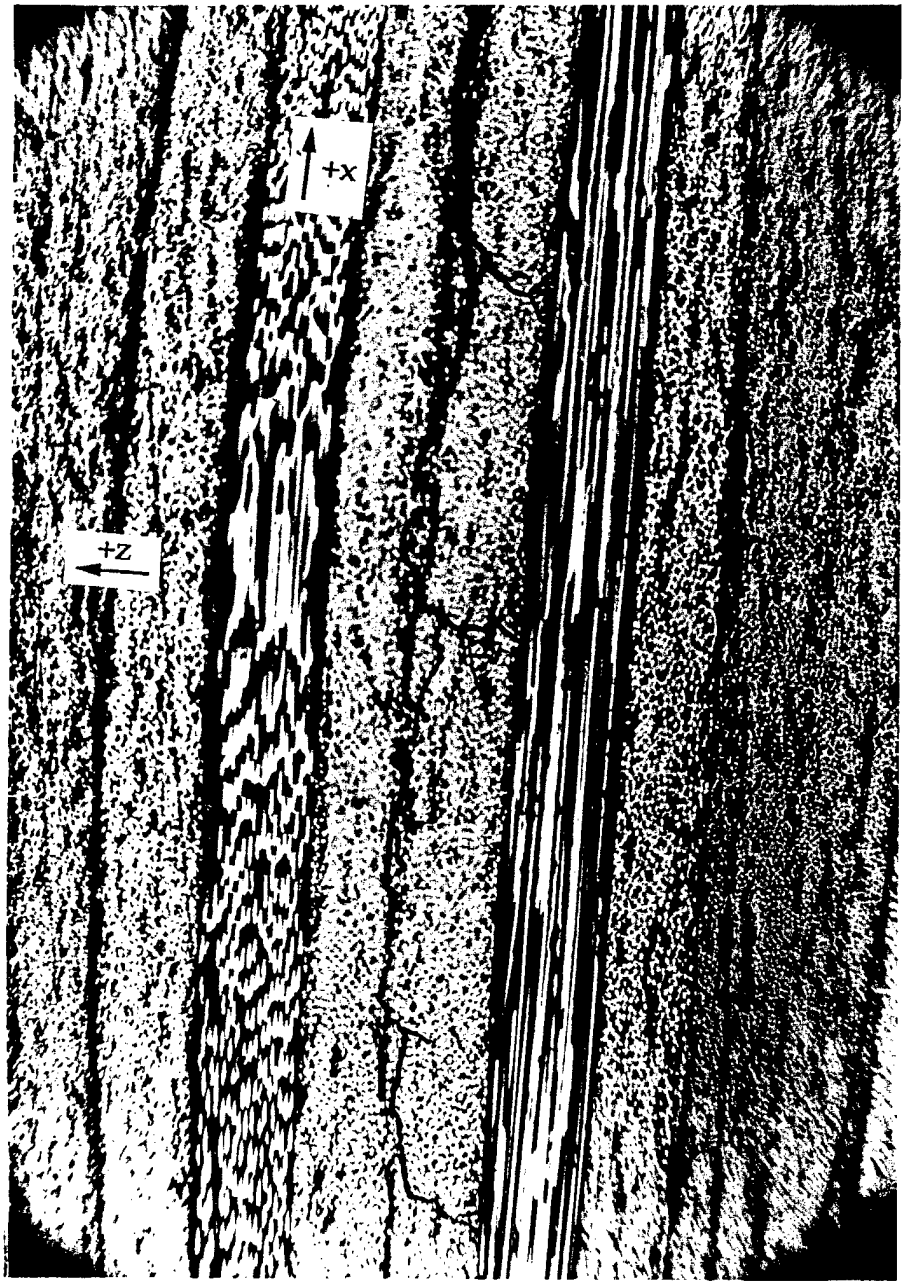

Figure 30.[en] Delamination propagation on the negative edge.

4.2.3. Observations on the Plate Face

In order to gain added insight into the nature of the damage development across the width of the plate, some of the case 2 specimens were also observed on the plate face. Two different techniques were used for these observations: *in situ* microscopic inspection and post-mortem penetrant-dye inspection.

4.2.3.1. Microscopic Inspection

The testing apparatus was modified so that the microscope could be kept perpendicular to the plate face as the specimen orientation changed during the test. The apparatus also provided the ability to move the microscope within the plane of the plate, as it did for the edge observations.

Microscopic inspection of the plate face was actually first employed in observing some of the specimens with 90° plate interface plies. However, the surface of the plate was imprinted with a weave pattern from one of the bleed clothes used during curing (a 90/0 cross weave). Since one of the weave directions coincided with the crack orientation, there was insufficient contrast to discern a crack on the rough surface of the plate face.* One of these specimens with a 90° plate interface ply was even tested by observing the edge surface until some large cracks appeared. The crack locations were then marked and the specimen face was inspected. However, the cracks could still not be seen on the face.

* This surface could not be polished because of the presence of the step.

The 45° orientation of the plate interface ply in case 2 specimens made them better suited to observations of the plate face since cracks oriented at 45° provided more contrast against the weave pattern (Figure 31). When a case 2 specimen was tested in this way, several cracks were able to be identified scattered across the width of the plate. These cracks were all oriented at 45° and were believed to originate by the step since two of them were seen to start by the step and then propagate away from it as the load increased. However, the crack which ultimately led to failure was not seen previously, indicating that the final fracture of the 45° ply on the $+x$ side of the step often occurs while the specimen is already in the process of failing catastrophically.

4.2.3.2. Penetrant-Dye Inspection

Several of the case 2 specimens were inspected post-mortem using penetrant dye.† The dye was applied to the top face of the plate near the step to learn more about the development of cracking in the 45° plate interface ply. The results of this inspection clearly showed that the cracks were scattered across the width of the specimen near the step. By comparing the cracks in a specimen that was not tested to catastrophic failure (Figure 32a) to one which had failed (Figure 32b), one can see that the cracks become more numerous as the test progresses. Also, inspection of one specimen which was tested only to

† Penetrant dye inspection is a relatively simple technique and is performed in the following steps:
1. The inspection surface is cleaned with a special solvent.
2. The dye is sprayed on after the specimen dries.
3. After allowing about 10 minutes for the dye to penetrate any surface cracks, the excess dye is removed with a cloth moistened with the cleaning solvent.
4. A developer is sprayed on, which turns white and draws the dye out of the cracks, forming red lines.

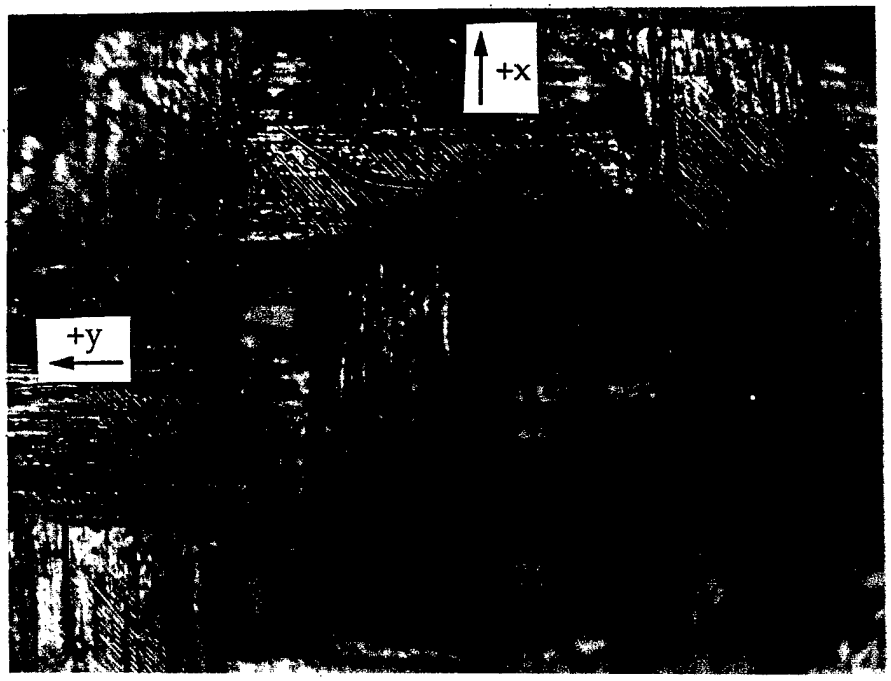

Figure 31. 45° crack on the plate face.

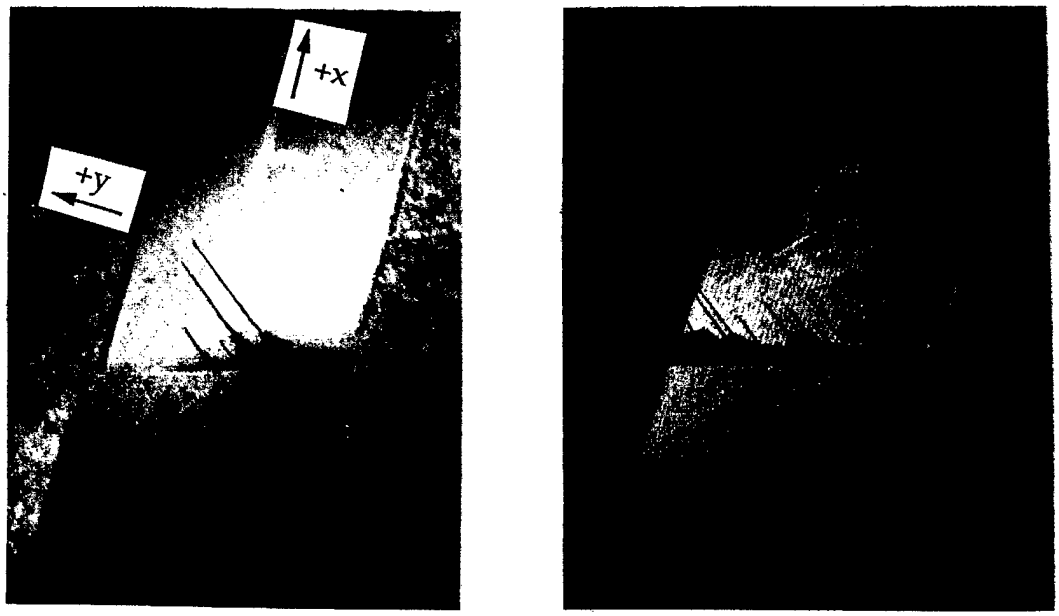

(a) (b)

Figure 32.[en] Penetrant-dye inspection of the plate face.
(a) prior to catastrophic failure. (b) after catastrophic failure.

the point of delamination initiation showed no cracks in the 45° plate interface ply. This observation indicated that the delamination was, in fact, the only damage on the specimen.* Furthermore, as mentioned in Section 4.1, the fact that a C-scan could not reveal any damage on this specimen verified that the delamination was localized to a small part of the step by the negative edge.

4.2.4. Overall Damage Process

Since many of the mechanisms involved in the case 2 damage development are similar to those discussed previously for cases 1 and 4, only the differences will be noted here. The main difference is associated with the location of the initial damage. Recall that for cases 1 and 4, the first damage to appear was transverse matrix cracking of the 90° plate interface ply near the step. However, for the case 2 lay-up, the damage begins as delamination of the 45/45 interface at the intersection of the step and the negative edge. In this case the damage initiation is dominated by the stress concentration at the corner. The primary reason for this dominance is believed to be the added/resolved strength of the 45° plate interface ply in the x direction. Since the fibers carry more of the load, the matrix-normal stress in the 45° ply does not become large enough to create a crack before the stress on the 45/45 interface exceeds its critical level.

---

* However, it is possible that there were matrix cracks in the 45° ply contained within a very small distance of the step. This is because there is a thin strip of the specimen near the corner in which the excess dye cannot be completely wiped away. When the developer is applied, this area becomes saturated with dye, preventing any damage from being seen there.

The delamination initiation mechanism is also different for the case 2 lay-up. For cases 1 and 4 delamination initiation was caused by the high interlaminar shear stress near the intersection of the 90° and 45° matrix cracks. However, for case 2 the interface usually begins cracking before any cracks appear in the adjoining plies. Thus, a region of high shear stress is not created by the presence of previous damage in the case 2 specimens. Instead, the delamination initiation is governed by the stress concentration that arises in the specimen's undamaged configuration.

Shortly after the delamination begins at the negative edge, matrix cracks begin developing in the 45° plate interface ply.* Although there seems to be a preference for the first few cracks to initiate closer to the negative edge (perhaps because of specimen twist), these cracks are soon distributed across the width of the specimen (Figures 32a and 32b). Since the cracks propagate away from the step on a 45° angle, the first crack to appear on the positive edge is usually a few ply thicknesses away from the corner. Also, this propagation direction prevents any of the cracks from intersecting the negative edge at positive values of x. Therefore, when viewing the negative edge, the only damage seen is that associated with delamination.

As the load increases, the delamination crack grows in the same way it did for case 1 and 4 specimens. The only difference is that for this lay-up, the initial delamination is on the 45/45 interface instead of the 90/45 interface. As before, when a sufficiently large portion of the specimen is delaminated,

* In one specimen matrix cracking in the 45° ply was believed to start before the delamination. This was the specimen in which damage was heard before the interface crack was seen on the negative edge. However, the 45° ply cracking must have been localized to the step area since it was not able to be detected using penetrant dye inspection.

the stress at the tip of the most recent crack across the 45° ply becomes large enough to kink the crack along the 45/0 interface, leading to catastrophic failure.

However, there is a significant difference between the final fracture surface of case 2 and case 1/4 specimens. Recall that for cases 1 and 4, the final fracture on the positive edge was always within a couple of ply thicknesses of the corner. However, of the case 2 specimens tested, the fracture surface extended between 0 and 22 ply thicknesses in the $+x$ direction from the corner. This difference is due to the absence of the 90° plate interface ply in case 2 specimens. This lay-up allows the 45° ply to separate freely from the plate below it (-z direction) at positive values of x. Thus, since in case 2 specimens less energy is required to separate the 45° ply where x is greater than zero, the fracture surface on the positive edge is usually located "farther away from the corner."

4.3. Lay-up Case 3

As for the other lay-ups, this section delineates the damage development of case 3 specimens. In this lay-up, the damage has to cross only the 90° plate interface ply before it gets to the top surface of the 0° ply, where unstable delamination occurs.* Therefore, since +45° or -45° plies are not primarily (directly) involved in the damage process, the final fracture surface

* In a static flexure test, the final delamination always occurs on the top surface of the upper 0° ply since the tensile stresses caused by bending are high enough to propagate cracks through the matrix in the 90° and 45° plies, but not through the 0° ply. The higher axial strength of the 0° ply causes the crack to kink in the direction of the interface, where it can continue to propagate without breaking any fibers.

is symmetric about the x-z plane. For this reason, the damage development is essentially the same when viewed from either edge, making it unnecessary to devote a section to each edge in describing the damage events. Since all case 3 specimens tested were observed on the positive edge,† the following section describes the features of the damage development as it occurred on that edge. As before, the loadings for one of the specimens have been included at each step to provide added insight into the size of the intervals between the various stages.

4.3.1. Observations on the Positive Edge

Each level of damage development seen on the positive edge is illustrated in Figure 33 and described in the steps which follow.

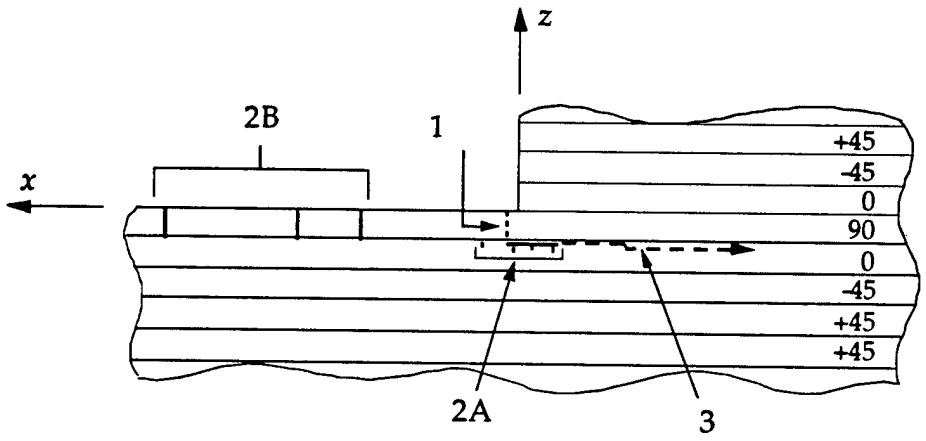

Figure 33. Damage development on the positive edge.

† Actually, a couple of the specimens were observed on the plate face, but since the damage was not seen before the specimens failed catastrophically, these tests proved to be of little value.

1. {$M \approx 45\%$ of M_{fp}} As in the case 1 and 4 tests, the damage process begins with a crack in the 90° ply near the step. However, for this lay-up the crack tends to be located closer to the corner (on average, about $\frac{1}{4}$ of a ply thickness from the corner).

2. {$M \approx 95\%$ of M_{fp}} At sufficiently high local loading, the corner crack turns in the $-x$ direction and propagates stably along the interface. As this happens, several fractures appear in the nearby 0° fibers ("2A" in Figure 33).

   At approximately the same loading, additional cracking develops in the plate interface ply at larger values of x ("2B" in Figure 33). However, at no point in the test do these cracks appear more severe than the damage by the corner.

3. {$M = M_{fp}$} Finally, the delamination which started in the previous step becomes unstable, leading to catastrophic failure. Again, the delamination crack often moves into the 0° ply as it travels toward the end of the specimen.

4.3.2. Overall Damage Process

Because of the absence of fracture in the ±45° plies, the damage observations for this lay-up are much easier to interpret. The tensile stress which is due to bending in the 90° ply first causes the plate interface ply to fail near the corner (where the stress is a maximum). This crack then arrests when it reaches the 0° ply. At higher loads, the stress becomes high enough at

the crack tip to kink the crack along the interface, which eventually leads to catastrophic failure.

However, there are two features about this damage process that are not immediately obvious. First, the tendency of the corner crack to develop closer to the step should be explained. It is believed that the higher axial stiffness of the 0° stringer interface ply in this lay-up causes a higher stress concentration at the corner. Similarly, the 90° stringer interface ply in case 1 and 4 specimens provides more flexibility near the corner and lessens the effect of the step. The higher stress concentration in case 3 specimens allows the geometric discontinuity to play a larger role in determining the location of fracture, causing the first crack to appear closer to the corner.*

The other feature which warrants further discussion is that stable delamination was observed on the positive edge. Since one of the causes of delamination propagation is believed to be the beam shear force, it may appear that the specimen is exhibiting stable behavior under an unstable process (Figure 16). However, even though the ±45° plies are not directly involved in the fracture process, they still cause the specimen to twist. Because the -45° plies are located farther from the neutral surface than the +45° plies (this ordering is the opposite of the other lay-ups), the highest curvature is at the positive edge. This means that the delamination initiates at the positive edge and that an increasing amount of new surface area must be created as the crack advances, until it has propagated across to the negative edge. Hence, the energy required to propagate the crack also increases. This

* This hypothesis is supported by Kubr's results for case 1 and 3 specimens. The severities (the values of k in the asymptotic form of the stress components, $\sigma = \psi r^{-k}$) for case 3 are about 4% higher than those of case 1.

increasing energy requirement is what allows the interface crack to propagate stably in the early stages of delamination on the positive edge.

4.4. The Effect of Stacking Sequence on Failure

This section attempts to make some general statements about how the failure process depends on the lay-up. Although it is difficult to draw any firm conclusions about this dependence from this limited study of only 3 lay-up cases (cases 1 and 4 are essentially the same), there are a few plausible deductions that can be made. It should be pointed out, though, that the following deductions apply only to the type of loadings considered in this experiment, i.e., when the stepped side of the plate is statically loaded in tension/bending.

The ply that seems to play the most important role in determining failure is the plate interface ply. If this ply has a low axial failure stress (90° orientation), it is likely that it will fail before the stress on the stringer–plate interface becomes large enough to cause failure by the corner. However, if this ply is relatively strong, it is likely that the stress on the stringer–plate interface will lead to failure.

Similarly, the plies below the plate interface ply influence the damage development through their contributions to the plate's bending strength (or stiffness). For the specimens tested, the failure-initiation loads (and catastrophic-failure loads) increase as the plate's bending stiffness increases.

The moment loadings at failure for the three lay-up cases with a .040" (1 mm) thick plate are shown in Table 2:

Lay-up	Failure Initiation Load (in.-lbs.)	Ultimate Failure Load (in.-lbs.)
1	-3.49	-8.98
2	-11.64	-16.57
3	-5.52	-12.26

Table 2. Average moment loadings at failure for lay-up cases 1, 2, and 3.*

This indicates that the strength of the plate-stringer combination is largely due to the strength of the outer few plies in the plate. Therefore, when designing a stepped composite plate (or stringer-reinforced plate) which will be subjected to the types of loadings considered in these tests, it seems desirable to choose a lay-up which offers very high bending stiffness in the x-z plane.

Although the effect of the stringer on the damage process is not clear, it seems that a stringer interface ply with a high axial stiffness allows the singularity to play the most significant role in the damage process. This hypothesis has arisen from a comparison of the damage development in case 1 (90° stringer interface ply) and case 3 (0° stringer interface ply) specimens. The first crack in case 3 specimens consistently appeared closer to the corner than the first crack in case 1 specimens, indicating that the stresses that were due to the singularity were higher in the case 3 lay-up.

* The average failure initiation load is computed from only the specimens which were observed on the edge associated with failure initiation (the negative edge in cases 1, 2, and 4; the positive edge for case 3). The average ultimate failure load is computed from all specimens which were tested to catastrophic failure.

In order to investigate this hypothesis further, some specimens were constructed with aluminum stringers. This was accomplished by bonding an aluminum strip onto the plate end of several case 1 and case 3 specimens. The objective of this procedure was to test some of the specimens with different stringers to see how extensively the stringer affected the damage process. However, these tests were unsuccessful because no adhesive of sufficient peel strength was found.

One other hypothesis regarding the stringer's effect on the damage process should be mentioned. It seems reasonable that a larger change in stiffness between the plate and the plate/stringer combination will cause the delamination-opening stresses to be higher. As mentioned earlier (Section 4.1.3), this discontinuous change in the bending stiffness contributes to the delamination propagation. Therefore, a larger stiffness change should yield larger delamination stresses. There are no data from this study to support or oppose this hypothesis. It is merely presented as an idea which can be investigated by other researchers in the future.

5. Comparison with Numerical Results

As mentioned previously, one of the goals of this study was to experimentally investigate the utility of Kubr's numerical results. This section evaluates how well those results agree with the failure behavior observed in the experiments.

5.1. Kubr's Failure Criterion

The most direct application of Kubr's work would be the use of his suggested failure criterion. Therefore, it is important to first determine how well this criterion predicts failure in the lay-up cases considered by this study. Since the criterion is based on a linearized solution about the (undamaged) reference configuration of the specimen, it only attempts to predict when damage *initiates* for a given lay-up. Therefore, the comparison with experimental observations should focus on damage initiation, possibly damage progression, but not catastrophic failure of the specimen.

In Section 4 an important feature of the damage initiation was revealed: Damage does not always occur on the stringer–plate interface as assumed by Kubr. This means that his failure criterion cannot possibly be used to predict damage initiation for arbitrary lay-ups. In fact, for the lay-ups tested in cases 1, 3, and 4, damage does not even occur right at the corner for every specimen. This observation is very important because it prevents the independent use of *any* criterion which is based on a similar singularity characterization.

For example, Kubr's characterization of the singularity was only concerned with stresses in a region between 10^{-8} and 10^{-6} mm away from the corner. However, in the case 1 and 4 specimens, the first damage occurred at distances between 1 t (.13 mm) and $1\frac{1}{2}$ t (.19 mm) away from the corner—over 5 orders of magnitude further away than the outer edge of the region considered by Kubr. There is no way that a criterion based solely on stress-intensity coefficients or severities calculated from this extremely small region can accurately predict failure which occurs several orders of magnitude further away from the corner. The state of stress away from the corner is no longer dominated by the character of the singularity. Therefore, it is not possible to accurately describe the stresses there solely from the information provided in a singularity characterization. A simple calculation can be performed to verify this fact: If Kubr's results are used to compare the relative stress levels (matrix-normal stress) at which failure occurs in a 90° plate interface ply (case 1, 3, or 4) and a 45° plate interface ply (case 2), the computed stress level at which the 45° ply fails is about 6 times higher than that for the 90° ply. This obviously is not correct since the matrix-normal strength should be the same in both plies.

It seems that for these lay-ups the damage is influenced more by the local variation in material parameters (fiber distribution, size and position of resin-rich areas, etc.) than by the precise structure of the singularity, as determined by a homogenized analysis. Therefore, since it is not known *a priori* where fracture will first occur in a specimen of arbitrary lay-up, a general failure criterion cannot assume that failure is governed solely by the character of the theoretical stress singularity. The nature of the singularity must be

considered in conjunction with other effects such as strength of the plate interface ply, stress concentrations due to local variations in material properties, and the ability of the material to redistribute loads away from regions of high stress.

The above discussion has illustrated the importance of experimentally verifying analytical or numerical work whenever feasible. This allows any shortcomings of the theories to be discovered and often provides additional insight which may be used to develop revised or new theories in the future.

5.2. Beam Calculations of Failure Strains

In order to further investigate how much the failure initiation was governed by the singularity, some approximate calculations were performed which estimate the failure strain of the plate interface ply based on uniform beam assumptions. These calculations totally neglect the presence of the stringer. They merely estimate the strain from the measured radius of curvature at failure. The purpose of these calculations is to explore the feasibility of a failure process which is dominated by classical bending stresses, and not by singularity stresses.

Under the assumptions that plane sections remain plane, one can derive the following expression for axial strain:

$$\varepsilon_{xx} = \frac{y}{R}\left(1+\varphi^2\right)^{\frac{3}{2}}\cos\varphi$$

where y is the distance above the mid-plane, φ is the angle of the beam at the point of interest (the deviation from the reference configuration),* and R is the radius of curvature. Using this formula and the experimental measurements, the axial failure strain of the plate interface ply was calculated for several specimens. This strain was then converted to matrix-normal strain, ε_{mm}, for the specimens with a 45° plate interface ply (case 2). Specimen twist was not accounted for in this conversion, i.e., $\varepsilon_{mm} = \frac{\sqrt{2}}{2}\varepsilon_{xx}$ was used. The results of these calculations are shown in Table 3.

Lay-up case	Plate interface ply	$\varepsilon_{m\,m}$
3	90°	.00351
1	90°	.00252
3	90°	.00242
2	45°	.00381
2	45°	.00439

Table 3. Failure strains of various plate interface plies.

The 90° ultimate strain of a unidirectional plate is .005. Therefore, the above procedure calculates failure strains which are lower than what one might expect, indicating that the singularity does indeed contribute to the failure process by raising the local stresses and strains. Also, this procedure tends to calculate higher failure strains for 45° plate interface plies than for 90° plate interface plies. This discrepancy is believed to be caused by the fact that curvature and angle measurements were taken when a crack was first seen on

* In the theory of strength of materials, φ is assumed to be small, allowing the expression to be simplified to $\varepsilon_{xx} = \frac{y}{R}$.

the positive edge. In a 45° plate interface ply the crack initiates inside the specimen so the loading is higher after the crack has propagated to the edge. This gives the appearance that the ply fails at a higher load.

Despite the inaccuracies in the above calculations, the uniform beam assumptions still yielded better estimates of the failure strains (or stresses) than Kubr's results.* This implies that failure initiation may actually be governed less by the singularity than by the bending stresses. It therefore seems logical that a future failure criterion should consider the possibility that failure may be caused by the nonsingular stresses in the plate interface ply, which can be described by uniform beam bending, as well as by the stresses on the stringer–plate interface, which are characterized by the singularity.

The fact that failure is not entirely governed by the nature of the singularity also has implications in finite-element modelling of composite structures. In several of the lay-ups tested (cases 1, 3, or 4), there was a significant variation in the damage initiation site. This variation indicates that the differences in stress, caused by changes in local material properties, occurs on a size scale which is a significant fraction of a lamina thickness. Thus, it seems that when creating a finite-element mesh, one cannot obtain any additional physically-relevant information about a singularity by generating an extremely fine mesh.†† Therefore, there does not seem to be

---

* Recall that calculations based on the results of Kubr's singularity characterization yielded failure stresses that differed by a factor of 6 for the two orientations of the plate interface ply.

†† It can also be argued that because of the continuum assumptions of a homogenized analysis, one cannot obtain any additional resolution in the stress field by using elements whose size approaches (or is less than) a fiber diameter.

any value in using elements smaller than approximately one-tenth of a lamina thickness.

5.3. Applying Kubr's Results to Lay-up Case 2

Since the first damage in lay-up case 2 occurred on the stringer–plate interface at the corner, one would expect the stresses at failure initiation to be well described by Kubr's analysis. This section attempts to use his numerical solution to predict the observed damage initiation.

From the results of Kubr's computations for case 2, the relative stress levels can be obtained on the 45/45 interface near the corner.† One should then be able to compare these stress levels with the appropriate material strengths (longitudinal interlaminar shear, transverse interlaminar shear, interlaminar tensile, and in-plane matrix-tensile strengths) to see which component of stress is responsible for damage initiation. However, the interlaminar strengths are not easily obtained. Even though there is no change in fiber orientation across the 45/45 interface being considered here, the higher concentration of voids, resin, and impurities on the interface gives it different properties than the material next to it. For this reason, it is not considered acceptable to calculate the interlaminar strengths from uniaxial strength equations, as given by Weeton et al. [1987].†† Since these equations

† Recall that Kubr characterized the stresses near the singularity in terms of their intensity coefficients, Ψ_{ij}, and their severities, k_{ij}: $\sigma_{ij} = \Psi_{ij} r^{-k_{ij}}$. It turns out that for the case 2 lay-up, the severities are approximately the same for all stress components. Therefore, the normalized stress-intensity coefficients can be used to provide a relative comparison of the various stresses.

†† In fact, if one calculates the various strengths from these equations, and then compares the ratios of each stress component to its corresponding strength, it turns out that the in-plane matrix-normal stress is the critical component in the interface region near the corner.

don't actually account for the presence of the interface, the interlaminar strengths will tend to be overestimated. Unfortunately, an adequate treatment of the interfacial effects on interlaminar strength could not be found. Therefore, it is not clear if the results from Kubr's numerical work can be used to predict damage initiation accurately for this lay-up.

This would predict a transverse matrix crack as the first damage to occur in a case 2 specimen (assuming the damage initiates in the region which lies directly in the $-x$ direction from the corner). This prediction conflicts with experimental observations, where the first crack appeared on the interface.

6. Concluding Remarks

6.1. Summary of Experimental Findings

In an attempt to further the understanding of the failure process in co-cured, stringer-reinforced composite plates and shells, an experimental investigation has been performed on the generic problem of a stepped composite plate. In addition to providing detailed descriptions of the damage process and insights into many of the mechanisms involved, this study sought to evaluate a failure criterion which was proposed in a recent numerical study of the same problem by Kubr. The present study used *in situ* microscopic inspection of the free edges to describe the damage development in specimens of 4 different lay-up cases. These observations were supplemented by penetrant-dye inspection, microscopic inspection of the plate face, and ultrasonic C-scanning.

The damage initiation site seems to be strongly dependent on the axial strength of the plate interface ply. If this ply is quite strong in the axial direction, as in a 0° or 45° orientation (case 2), failure begins on the stringer–plate interface by the corner. However, if this ply is oriented at 90° (cases 1, 3, and 4), it fails before the loads at the corner become high enough to fracture the interface. In this latter case, the first damage to appear is transverse matrix cracking in the plate interface ply. Not only is this damage initiation not on the stringer–plate interface, as is often assumed, but the damage in many specimens occurs more than a lamina thickness away from the singularity. This observation is quite significant because it indicates that Kubr's failure criterion, or any failure criterion based solely on the character

of the singularity, cannot accurately predict failure in specimens of arbitrary lay-up.

6.2. Suggestions for Future Research

A detailed explanation of the suspected damage mechanisms has been presented in this thesis to aid future researchers in developing a comprehensive understanding of the damage process. However, additional work is required either to verify or refute many of the ideas presented here. Future experiments could be designed specifically to evaluate these hypotheses, or the validity of the hypotheses could be reassessed after a broader base of experimental evidence has been developed.

The current study has observed the progression of damage in specimens which were statically loaded with the stepped side of the plate in tension. It would also be beneficial to conduct fatigue tests or similar static tests with the stepped side loaded in compression. The observations of the damage development under a wide variety of loadings could provide valuable insights into the failure behavior of parts subjected to their service loadings.

Since only 4 different lay-up cases were studied in this experiment, it is difficult to draw many conclusions about the effects of stacking order on the failure process. Therefore, it would be useful to expand the test matrix to include several other lay-ups. This should provide additional insight into ways of optimizing the stacking sequence to allow the specimen to support

higher loadings at the step. It is possible that this information could then be used to improve the strength of composite structures without compromising stiffness or manufacturing costs.

Finally, this work has provided experimental observations whose consideration should allow more accurate failure criterions to be developed in the future. These criterions may be based on numerical or analytical estimates of the stresses, but they must not assume that failure initiation for all lay-ups will occur in the same location.

References

Bogy, David B. (1968), "Edge-Bonded Dissimilar Orthogonal Elastic Wedges Under Normal and Shear Loading," *J. App. Mech.*, vol. 40, pp. 460-466.

Brockenbrough, J.R., Suresh, S., and Wienecke, H.A. (1991), "Deformation of Metal-Matrix Composites with Continuous Fibers: Geometrical Effects of Fiber Distribution and Shape," *Acta Metall. Mater.*, vol. 39, pp. 735-752.

Broek, David (1986), *Elementary Engineering Fracture Mechanics*, Kluwer Academic, Dordrecht, The Netherlands.

Freeman, S.M. (1982), "Characterization of Lamina and Interlaminar Damage in Graphite/Epoxy Composites by the Deply Technique," *Composite Materials: Testing and Design (Sixth Conference), ASTM STP 787*, I.M. Daniel, Ed., American Society for Testing and Materials, pp. 50-62.

Gustafson, C.G. and Seldén, R.B. (1985), "Monitoring Fatigue Damage in CFRP Using Acoustic Emission and Radiographic Techniques," *Delamination and Debonding of Materials, ASTM STP 876*, W.S. Johnson, Ed., American Society for Testing and Materials, Philadelphia, pp. 448-464.

Hein, V.L. and Erdogan, F. (1971), "Stress Singularities in a Two-Material Wedge," *Int. J. Fract. Mech.*, vol. 7, pp. 317-330.

Hillman, D.J. and Hillman, R.L. (1985), "Thermographic Inspection of Carbon Epoxy Structures," *Delamination and Debonding of Materials, ASTM STP 876*, W.S. Johnson, Ed., American Society for Testing and Materials, Philadelphia, pp. 481-493.

Hogarth, C.A. and Blitz, J. (1960), *Techniques of Non-Destructive Testing*, Butterworths, London.

Kellas, S., Morton, J., and Bishop, S.M. (1985), "Damage Development in Notched Carbon Fiber Composites Subjected to Fatigue Loading," *Composite Structures 3*, I.H. Marshall, Ed., Elsevier Applied Science, London, pp. 56-68.

Kubr, Thomas J. (1990), "Stresses Near a Change of Thickness in a Continuous-Fiber-Composite Plate," Ae.E. Thesis, Caltech, Pasadena, CA.

Lekhnitskii, S.G. (1963), *Theory of Elasticity of an Anisotropic Elastic Body*, Holden-Day, San Francisco.

Marr, G.R., Barrowcliffe, R.P., and Curtis, A.R. (1985), "The Non-destructive Evaluation of Composite Bonded Joints," *Composite Structures 3*, I.H. Marshall, Ed., Elsevier Applied Science, London, pp. 502-510.

Mignery, L.A., Tan, T.M., and Sun, C.T. (1985), "The Use of Stitching to Suppress Delamination in Laminated Composites," *Delamination and Debonding of Materials, ASTM STP 876,* W.S. Johnson, Ed., American Society for Testing and Materials, Philadelphia, pp. 371-385.

Pogue, William R. III and Vizzini, Anthony J. (1989), "Structural Tailoring Techniques to Prevent Delamination in Composite Laminates," *American Helicopter Society, 45th Annual Forum Proceedings,* Boston, MA, pp. 489-496.

Ratwani, M.M. and Kan, H.P. (1982), "Effect of Stacking Sequence on Damage Propagation and Failure Modes in Composite Laminates," *Damage in Composite Materials, ASTM STP 775,* K.L. Reifsnider, Ed., American Society for Testing and Materials, Philadelphia, pp. 211-228.

Stevanovic, M.M., Briski, D.B., and Kostic, M.C. (1985), "Mechanical Properties and Fractographic Examination of Failure Created in Static Mechanical Testing of CFRP," *Composite Structures 3,* I.H. Marshall, Ed., Elsevier Applied Science, London, pp. 369-382.

Tsai, Stephen W. and Hahn, H. Thomas (1980), *Introduction to Composite Materials,* Technomic, Westport, CT.

Vinson, J.R. and Sierakowski, R.L. (1987), *The Behavior of Structures Composed of Composite Materials,* Kluwer Academic, Dordrecht, The Netherlands.

Waas, Anthony M. (1987), "Compression Failure of Fibrous Laminated Composites in the Presence of Stress Gradients: Experiment and Analysis," Ph.D. Thesis, Caltech, Pasadena, CA.

Wang, S.S. and Choi I. (1982), "Boundary-Layer Effects in Composite Laminates: Parts 1 and 2," *J. App. Mech.,* vol. 49, pp. 541-560.

Weeton, John W., Peters, Dean M., and Thomas, Karyn L. (1987), *Engineers' Guide to Composite Materials,* American Society for Metals, Metals Park, OH.

Williams, M.L. (1952), "Stress Singularities Resulting from Various Boundary Conditions in Angular Corners of Plates in Extension," *J. App. Mech.,* vol. 19, pp. 526-528.

Williams, M.L. (1959), "The Stresses Around a Fault or Crack in Dissimilar Media," *Bulletin of the Seismological Society of America,* vol. 49, pp. 199-204.

Appendix

Principal Bending Axis Calculation for Case I Specimens

As mentioned in Section 4.1.3, composite materials in general exhibit coupling between bending and twisting. This is most easily seen by looking at the relation between moments and curvatures for a symmetric composite plate, neglecting thermal and hygrothermal (moisture) effects:

$$\begin{Bmatrix} M_x \\ M_y \\ M_{xy} \end{Bmatrix} = \begin{bmatrix} D_{11} & D_{12} & D_{16} \\ D_{12} & D_{22} & D_{26} \\ D_{16} & D_{26} & D_{66} \end{bmatrix} \begin{Bmatrix} \kappa_x \\ \kappa_y \\ 2\kappa_{xy} \end{Bmatrix}.$$

By looking at the components of $\boldsymbol{D}$, the flexural stiffness matrix, one can see that the presence of nonzero D_{16} and D_{26} terms indicates coupling between bending and twisting. The components of the $\boldsymbol{D}$ matrix can be calculated from material properties and stacking sequences, as will be shown later.

Where this appendix was referenced on page 40, a hypothesis was presented which stated that the delamination crack front coincides with the principal bending axis. Since the objective of this appendix is only to investigate the plausibility of this hypothesis, we need only get a rough approximation of the orientation of the axis. Recall that for case 1 specimens, the delamination begins on the 90/45 interface. Therefore, since the 90° ply has little effect on the bending stiffness or twisting behavior, the plate below the delamination has approximately the same bending-twisting coupling as the stringer and 90° ply above the delamination.† For this reason the

† Recall that the plate and stringer have the same lay-ups for case 1.

delamination crack-front angle can be approximated by the angle of the plate's principal bending axis.* This makes the following calculations much simpler since it is not necessary to account for the presence of the stringer, and it is not necessary to use the more complicated constitutive relations of an asymmetric plate, which has extensional-bending coupling as well as bending-twisting coupling.

As described in Section 4.1.3, the principal bending axis of a plate is the axis about which it bends when subjected to a nontorsional loading. Therefore, in order to find the orientation of this axis, one must find the frame in which the bending-twisting coupling disappears. This frame corresponds to the principal frame of the flexural stiffness matrix. However, before the principal frame can be determined, the components of D must first be calculated in the x-y coordinate system.

Following the notation of Vinson and Sierakowski [1987], the components of D are given by

$$D_{ij} = \frac{1}{3}\sum_{k=1}^{N}\left(\overline{Q}_{ij}\right)_k\left[h_k^3 - h_{k-1}^3\right],$$

* It should be understood that this becomes a bigger assumption when the delamination moves to the 45/0 interface. At this point the delamination becomes more complicated, as explained on pages 47-50. Even though the portion of the plate near the tip of the delamination crack no longer contains the 45° ply, the ply still affects the orientation of the crack front. This is because the 45° ply remains attached to the plate on the $+x$ side of the step and the stringer on the delamination surface, prohibiting the delamination crack from opening as it would without the 45° ply.

However, it should be emphasized again that this appendix is not intended to provide a precise model of the twisting of the specimen portions above and below the delamination surface. Its only purpose is to get a crude approximation of the delamination front orientation based on the assumption that it is controlled by the orientation of the principal bending axes. One can then see if this approximation is anywhere near the observed delamination front.

where $(\overline{Q}_{ij})_k$ are the components in the x-y coordinate system of the matrix relating stress and strain for the kth ply; h_k is the vectorial distance from the laminate midplane to the upper surface of the kth lamina, i.e., positive above the midplane and negative below it; and N is the number of plies in the plate. The components of $\overline{Q}$ are functions of the material properties and orientation of the kth ply. Specifically, the components of interest here are given by

$$\begin{aligned}
\overline{Q}_{11} &= Q_{11}m^4 + 2(Q_{12} + 2Q_{66})m^2n^2 + Q_{22}n^4 \\
\overline{Q}_{12} &= (Q_{11} + Q_{22} - 4Q_{66})m^2n^2 + Q_{12}(m^4 + n^4) \\
\overline{Q}_{16} &= -mn^3Q_{22} + m^3nQ_{11} - mn(m^2 - n^2)(Q_{12} + 2Q_{66}) \\
\overline{Q}_{22} &= Q_{11}n^4 + 2(Q_{12} + 2Q_{66})m^2n^2 + Q_{22}m^4 \\
\overline{Q}_{26} &= -m^3nQ_{22} + mn^3Q_{11} + mn(m^2 - n^2)(Q_{12} + 2Q_{66}) \\
\overline{Q}_{66} &= (Q_{11} + Q_{22} - 2Q_{12})m^2n^2 + Q_{66}(m^2 - n^2)^2,
\end{aligned}$$

where $m = \cos\theta$, $n = \sin\theta$, and θ is the ply orientation as described in Figure 4. The Q_{ij} quantities are the components of the stiffness matrix in the material coordinate system (the principal coordinate system of a unidirectional plate) and are identical to the C_{ij} quantities of classical elasticity. The components of interest can be approximated as

$$\begin{aligned}
Q_{11} &= \frac{E_{11}}{1 - \nu_{12}\nu_{21}} \\
Q_{22} &= \frac{E_{22}}{1 - \nu_{12}\nu_{21}} \\
Q_{12} &= \frac{\nu_{12}E_{22}}{1 - \nu_{12}\nu_{21}} = \nu_{12}Q_{22} \\
Q_{66} &= G_{12}.
\end{aligned}$$

Here the subscript 1 denotes the fiber direction, while the subscript 2 denotes the in-plane direction perpendicular to the fibers. The above material

parameters are all known or can be easily calculated. In agreement with standard convention, Poisson's ratio is defined as

$$\nu_{ij} = -\frac{\varepsilon_{jj}}{\varepsilon_{ii}} \qquad \text{(no sum)},$$

where the applied stress is in the x_i direction. All of the material parameters except ν_{21} are given in Table 4:

E_{11}	20.5 x 10^6 psi	Tensile stiffness in the fiber direction
E_{22}	1.67 x 10^6 psi	Tensile stiffness in the matrix direction
G_{12}	.87 x 10^6 psi	Shear modulus
ν_{12}	.3	Major Poisson's ratio
ρ	.057 lbs./in^3	Density
$(\varepsilon_{11})_y$	.00653	0° limit strain (tension)
$(\varepsilon_{22})_{ult}$	.005	90° ultimate strain (tension)

Table 4. Room temperature material properties of unidirectional A34/3502.

The value of ν_{21} is calculated from the relation

$$\nu_{21} = \frac{E_{22}}{E_{11}}\nu_{12}.$$

Therefore, all of the information needed to calculate **D** for a given laminate is now known. For the case 1 laminate* that we are interested in we can use its symmetry to reduce the amount of calculation required. In a symmetric laminate we need only sum the contributions of the plies on one

* Recall that the case 1 lay-up is $[90/+45/0/-45]_S$, where each ply is about .005" thick.

side of the midplane and then multiply by 2 to get the values of D_{ij}. Therefore, for our laminate we have

$$D_{ij} = \frac{2}{3}\sum_{k=1}^{4}\left(\overline{Q}_{ij}\right)_k\left[h_k^3 - h_{k-1}^3\right].$$

These calculations are quite long and tedious, so they will be omitted here. The results are:

$$[\mathbf{D}] = \begin{bmatrix} 29.047 & 10.347 & 7.305 \\ 10.347 & 75.551 & 7.113 \\ 7.305 & 7.113 & 11.857 \end{bmatrix}.$$

Since D_{16} and D_{26} are nonzero, the plate exhibits bending-twisting coupling in this reference frame, as expected. In order to find the principal frame of **D**, where this coupling disappears, one must simply find its eigen vectors. After completing the eigen-value problem, the eigen vectors are found to be:

$$\{\mathbf{u}_1\} = \begin{Bmatrix} .922 \\ -.248 \\ .297 \end{Bmatrix} \qquad \{\mathbf{u}_2\} = \begin{Bmatrix} .220 \\ .967 \\ .127 \end{Bmatrix} \qquad \{\mathbf{u}_3\} = \begin{Bmatrix} -.318 \\ -.052 \\ .947 \end{Bmatrix}.$$

By defining β to be the angle between the y axis and the projection of the second principal axis onto the x-y plane, one can approximate the orientation of the principal bending axis:

$$\beta = \tan^{-1}\left(\frac{.220}{.967}\right) = 12.8°.$$

When this is compared to the orientation of the delamination crack front for the case 1 specimen in Figure 20, one finds that the agreement is very good. The delamination crack front in Figure 20 is oriented at 11.3° from the step. This agreement indicates that the presumed hypothesis is quite plausible.

Therefore, it is likely that the delamination crack front is parallel to the principal bending axis.